JOURNAL OF GEOPHYSICAL RESEARCH, VOL. 95, NO. B8, PAGES 12,927–12,945, AUGUST 10, 1990

The Sound Field Near Hydrothermal Vents on Axial Seamount, Juan de Fuca Ridge

SARAH A. LITTLE

Department of Geology and Geophysics, Woods Hole Oceanographic Institution, Woods Hole, Massachusetts

KEITH D. STOLZENBACH

Department of Civil Engineering, Massachusetts Institute of Technology, Cambridge

G. MICHAEL PURDY

Department of Geology and Geophysics, Woods Hole Oceanographic Institution, Woods Hole, Massachusetts

High-quality acoustic noise measurements were obtained by two hydrophones located 3 m and 40 m from an active hydrothermal vent on Axial Seamount, Juan de Fuca Ridge, in an effort to determine the feasibility of monitoring hydrothermal vent activity through flow noise generation. Most of the measured noise field could be attributed to ambient ocean noise sources of microseisms, distant shipping, and weather, punctuated by local ships and biological sources. Long-period, low-velocity, water/rock interface waves were detected with high amplitudes which rapidly decayed with distance from the seafloor. Detection of vent signals was hampered by unexpected spatial nonstationarity due to the shadowing effects of the caldera wall. No continuous vent signals were deemed significant based on a criterion of 90% probability of detection and 5% probability of false alarm. However, a small signal near 40 Hz, with a power level of 10^{-4} Pa^2/Hz was noticed on two records taken within 3 m of the Inferno black smoker. The frequency of this signal is consistent with predictions, and the power level suggests the occurrence of jet noise amplification due to convected density inhomogeneities.

INTRODUCTION

At mid-ocean ridges the circulation of seawater brings heat and chemicals up from the depths of oceanic lithosphere, releases part of this load onto the seafloor, and injects the rest into the water column. The full impact of hydrothermal circulation on ocean composition, global heat flux, and generation of economic ore deposits has not been assessed because neither the full spatial nor temporal distributions of venting are known. Thirty or so vent sites of varying size have been identified both in the Pacific and Atlantic oceans since their first discovery in 1977 [*Corliss et al.*, 1979; *Hoagland and Broadus*, 1987]. Although instantaneous measurements of hydrothermal characteristics such as morphology, temperature, salinity, chemistry, heat flux, and biological composition have been taken at many of them [*Ballard et al.*, 1981; *Ballard et al.*, 1982; *Ballard et al.*, 1983; *Converse et al.*, 1984; *Craig et al.*, 1987; *Crane et al.*, 1985; *Francheteau and Ballard*, 1983; *Hammond et al.*, 1984; *Hekinian et al.*, 1983; *Hessler and Smithey*, 1983; *Little et al.*, 1987; *McConachy et al.*, 1986; *Macdonald*, 1983; *Normark et al.*, 1986; *Rona et al.*, 1986; *Tivey and Delaney*, 1986], long-term measurements of any type greater than a few days are extremely rare [*Johnson and Tunnecliffe*, 1985; *Little et al.*, 1988]. This deficiency is due to the inaccessibility and severe environmental conditions found at vents, for example, high temperatures, high pressures and reactive chemicals. An understanding of the local scale fluid flow characteristics and changes in these over time is required to develop models of hydrothermal processes ranging from subsurface water-rock interactions [*Cann and Strens*, 1982; *Cann et al.*, 1986] to biological dispersion and growth [*Hessler et al.*, 1985; *Van Dover*, 1986]. The current scientific need to remotely monitor long-term changes in flow velocity has justified a feasibility test of a passive acoustic monitor at a high-temperature vent field. This method utilizes the sound generated by moving fluid at hydrothermal chimneys, the frequency and amplitude of which depend upon the fluid velocity and density, orifice diameter, and chimney structure [*Lighthill*, 1952; *Dowling et al.*, 1978; *Ffowcs Williams*, 1969; *Morfey*, 1973].

In theory, an exact description of vent sound could be used to determine flow velocity, orifice diameter and possibly fluid density (Appendix A). In practice, however, no unequivocal proof exists that vents generate sound at levels that are detectable in the deep ocean, although some data are available that suggest that this is so (see below). No measurements of vent sound have been made of adequate quality to determine source mechanisms and to permit estimation of vent parameters. In this paper an experiment is described which was designed to determine the feasibility of detecting hydrothermally generated sound in the ocean. In September 1987, high-quality recordings of noise within a few tens of meters of an active vent were made using two hydrophones emplaced by the submersible *Alvin* in Ashes Vent Field, Axial Seamount, on the Juan de Fuca Ridge (45° 55'N, 30° 02'W). The results of this experiment are presented in this paper.

REVIEW OF AMBIENT OCEAN NOISE

The potential difficulty in detecting hydrothermal vent acoustic signals lies not so much in the sensitivity of hydrophones and recording instruments, as in the intensity and variability of ambient ocean noise. Typical, ubiquitous, deep-water ambient ocean noise spectra can be separated into four frequency bands caused by four different source mechanisms (Figure 1) [*Urick*, 1975; *Urik*, 1986; *Burdick*, 1984; *Wentz*, 1962].

The lowest-frequency band, 0.01-5 Hz, exhibits high power levels and is dominated by microseisms (low-frequency pressure disturbances caused by nonlinear interactions of ocean surface waves [*Webb*, 1984]), and teleseismic events. Temporal variations

Paper number 89JB03783.
0148-0227/90/89JB-03783$05.00

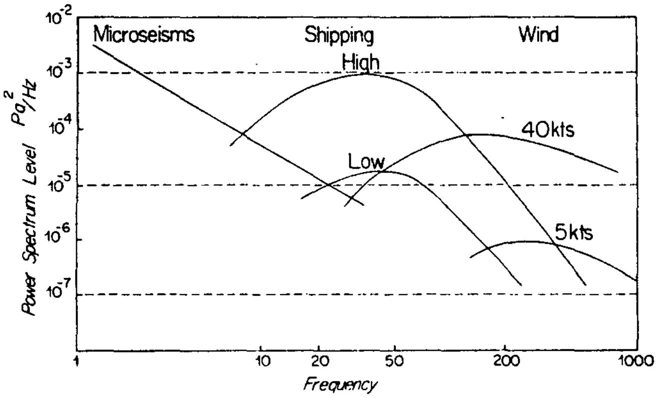

Fig. 1. Typical ambient ocean noise spectra [*Urick*, 1986]. Noise below 10 Hz is dominated by microseisms, between 10 and 200 Hz by shipping, and between 200 and 1000 Hz by weather.

are as rapid as a few minutes for interface waves travelling near the seafloor from teleseismic sources and as long as a few hours for variations in sea state and swell.

Power in the band from 5 to 100 Hz, produced by distant shipping, is dependent on sound that has travelled tens to hundreds of kilometers and is strongly influenced by wave-guide propagation effects such as sound channelling due to a velocity minimum. Travelling great distances through the ocean eliminates waves travelling outside a few degrees of horizontal. Time variations in this band are slow, of the order of hours to days and depend on changes in ship traffic and large-scale temperature and salinity structure (in the sound channel).

The midband, 100-10,000 Hz, is a function of local sea state and wind related noise caused by spray, breaking waves, and falling water droplets. Sound due to weather within a few kilometers of the measurement site will dominate pressure levels on the seafloor in this frequency band. Changes with time in power level are of the order of hours to days and are dependent on weather patterns.

Finally, the high-frequency band above 10,000 Hz is dominated by noise caused by thermal agitation of water molecules.

Transient sources also contribute to noise at a given location. These include local ships and submarines, which are characterized by high-energy narrow band peaks, often including harmonics of a fundamental frequency, anywhere from 5 to 200 Hz. Biological sources can contribute to the noise field, with whales and dolphins capable of producing high-amplitude, short-duration sounds at frequencies from 18 to 100 Hz [*Watkins*, 1981].

Noise in the ocean is typically nonstationary both in time and space [*Burdick*, 1984; *Hodgkiss and Anderson*, 1980]. The noise field varies considerably over time due to the rich variety of sources [*Akal et al.*, 1986] and measurements made hours apart can show striking dissimilarity (as will be seen below). Sound recorded at near-bottom hydrophones is subject to additional propagation effects of local topography, seafloor heterogeneity, and interface of the ocean-seafloor boundary. These effects can produce severe spatial variability in the sound field over short distances through diffraction, scattering, and exponential decay of interface waves with distance from a boundary. In the face of these difficulties, and to make the study of noise in the ocean tractable, the necessary assumption of stationarity is often validated by making comparisons over closely spaced times and distances.

Site Description

Ashes Vent Field [*Hammond et al.*, 1986] is located 75 m from the southwestern wall of Axial Seamount on the Juan de Fuca Ridge at 45° 55'N, 30° 02'W [*Canadian American Seamount Expedition (CASM)*, 1983; *Canadian American Seamount Expedition*, 1985; *Embley et al.*, 1988] (Figure 2). The site is noted for its smooth floor and absence of cracks and fissures, which makes it an ideal spot in which to work with the submersible and emplace a vertical instrumented cable. The caldera floor, approximately 4 km from east to west and 10 km north to south, is 1540 m below the sea surface which nominally places it in the deep sound channel for this latitude [*Burdick*, 1984]. In the Ashes Vent Field, there are two main black smokers with accompanying sulfide and anhydrite chimneys, "Hell" and "Inferno," separated by 35 m (Figure 3). In addition to these there are several lower-temperature and velocity white smokers and many patches of diffuse flow within the 60x60 m area of hydrothermal activity. At the time of acoustic sampling, the chimney of Inferno was 3 m high, topped by one site of black smoke efflux sampled at a temperature of 326° C with visually determined exit velocity of 1-2 m/s and diameter of 4 cm. There were, in addition, several other sites of clear fluid discharge, one located 20 cm from the black smoker, with a temperature of 126° C, velocity of less than 1 m/s, and diameter of 1 cm. The others were located near the bottom of the edifice. The chimney of Hell was 2 m high and hosted a single black smoker at its top with an orifice diameter of 5 cm and a visually estimated exit velocity of 0.5-1.5 m/s.

Instrumentation and Deployment

The hydrothermal acoustic monitoring instrument consisted of two hydrophones suspended on a cable beneath a float (Figure 4) and attached to a microprocessor-controlled digital recording system [*Mellinger et al.*, 1986]. Designed for detecting an unknown vent acoustic signature, the system had a 16-bit analog-to-digital converter and a programmable 1-10-100-1000 gain amplifier resulting in a dynamic range of 156 dB. One tunable eight-pole Butterworth filter for each channel provided antialiasing for sampling rates of 300 and 2400 Hz. Calibration to absolute sound power levels was obtained by comparison to a known receiver and is accurate to within 6 dB for the bandwidth 15-1200 Hz and 15 dB for the bandwidth 1-15 Hz. Calibration of relative response between the two channels revealed less than a 4-dB difference for all frequencies of interest (0.5-1200 Hz) in this experiment.

The deployment scheme was designed to accommodate three major constraints: minimizing the use of the submersible, recording without ships or submarines in the vicinity, and limited memory storage capability. To achieve this, the instrument was dropped from the ship and targeted on the vent site using an acoustic navigation net, then moved to within 5 m of an active chimney by the submersible *Alvin*. The instrument turned on at a preset time and recorded through the night after the submarine and ship had left the area. The following day, the instrument was acoustically released and recovered by the surface ship. The data were then transferred to a portable computer, and the instrument was readied for further deployments.

Data Description

Two fully successful hydrothermal acoustic monitor deployments were obtained on *Atlantis II*/*Alvin* voyage 118, leg 21. For the first deployment, *Alvin* dive 1917, the lower hydrophone was placed 2 m horizontally and 1 m vertically from the northeast side of black smoker Inferno. The upper hydrophone was 39.5 m above the lower one. The instrument turned on at 2100 LT on September 23, 1987 and recorded two consecutive sets of data every hour until 0300 LT on September 24, 1987. The first set was 9216 points long taken at 2400 Hz with antialias filter at 800 Hz. The second set was 8192 points long recorded at 300 Hz

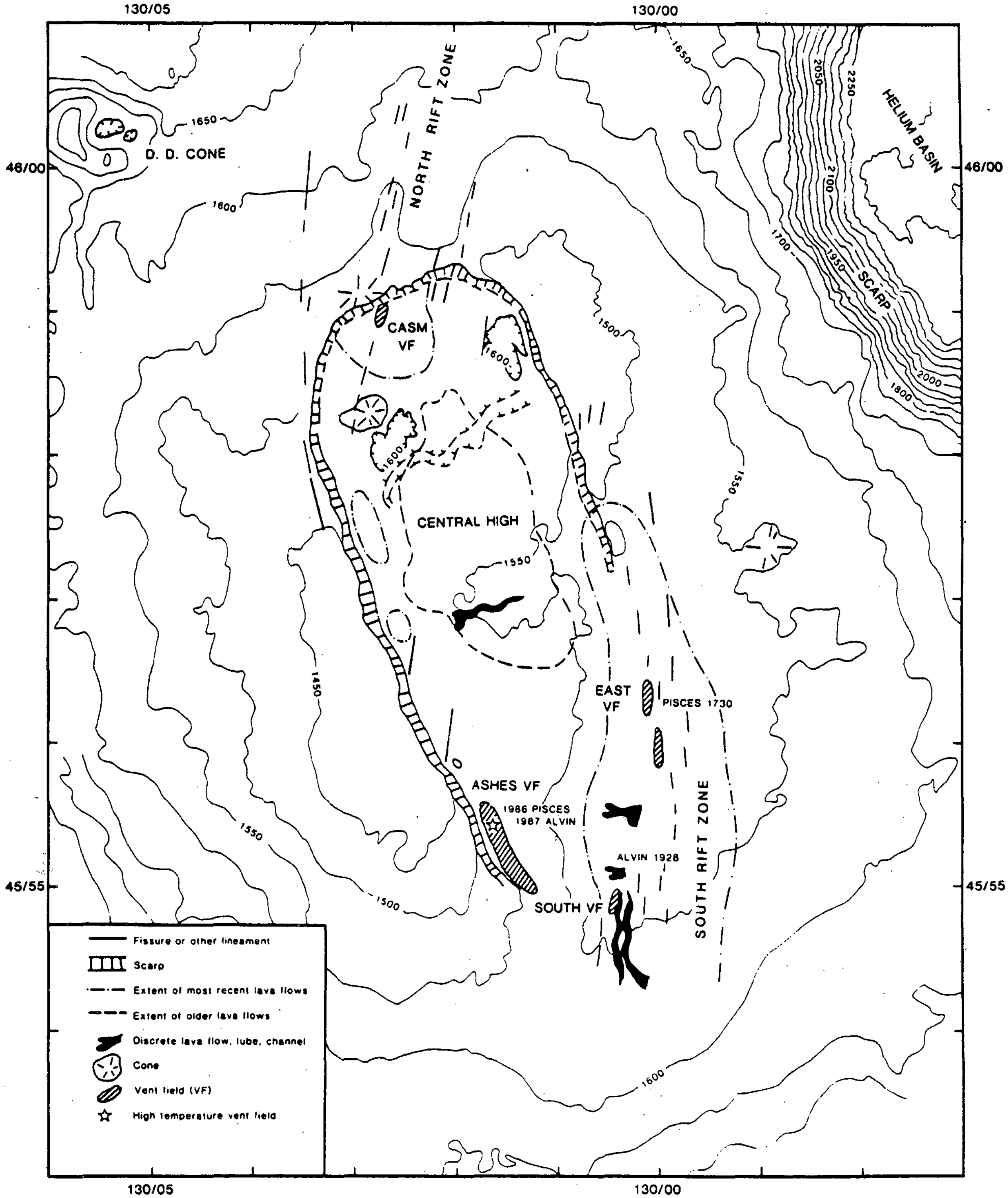

Fig. 2. Location of Ashes Vent Field in Axial Seamount, on the Juan de Fuca Ridge. The field is just east of the 50-100 m high scarp defining the caldera wall [*Embley et al.*, 1988]. An earlier seismic experiment had a hydrophone near CASM vent field in the northern part of the caldera.

with antialias filter at 100 Hz. A total of 14 sets were obtained, seven at each of the two frequencies.

On the second deployment the lower hydrophone was positioned 2 m horizontally and 2 m vertically above black smoker Hell, 35 m from Inferno, on dive 1923. The upper hydrophone was 38.9 m above the lower. The instrument began recording at 1800 LT on September 29, 1987 and sampled once an hour until 0600 LT on September 30,1987. Each sample was 8192 points long taken at 300 Hz with antialias filter at 100 Hz, for a total yield of 13 sets.

General Data Reduction

The output of a hydrophone placed in the ocean results from a combination of system noise and pressure fluctuations in the

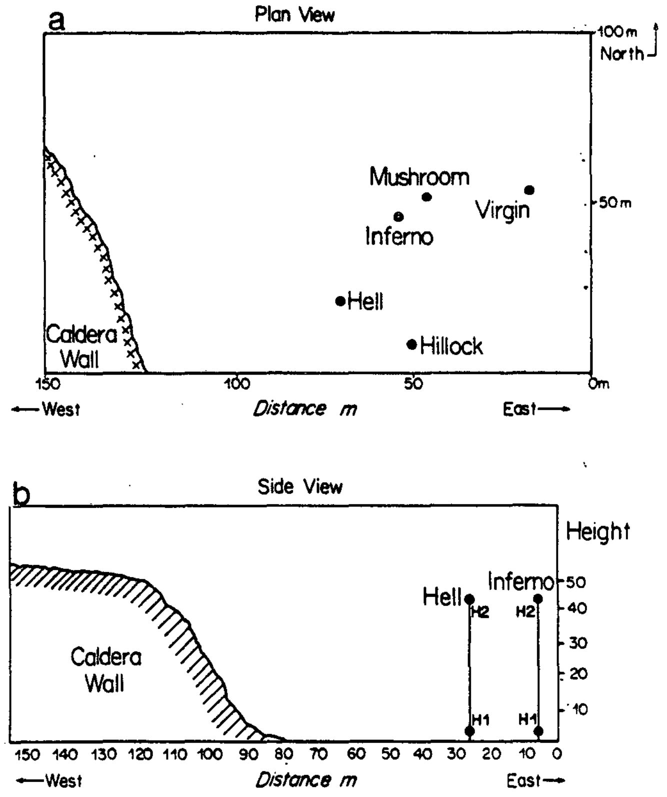

Fig. 3. (*a*) Plan view of Ashes Vent Field showing black smokers Hell and Inferno and white smokers Mushroom, Hillock, and Virgin Mound, with caldera wall 60-80 m to the west of deployment sites. (*b*) Side view of deployment showing relationship between wall, vents, and hydrophone array. Eastward travelling waves are prevented from reaching lower hydrophones by the shadowing effect of this wall.

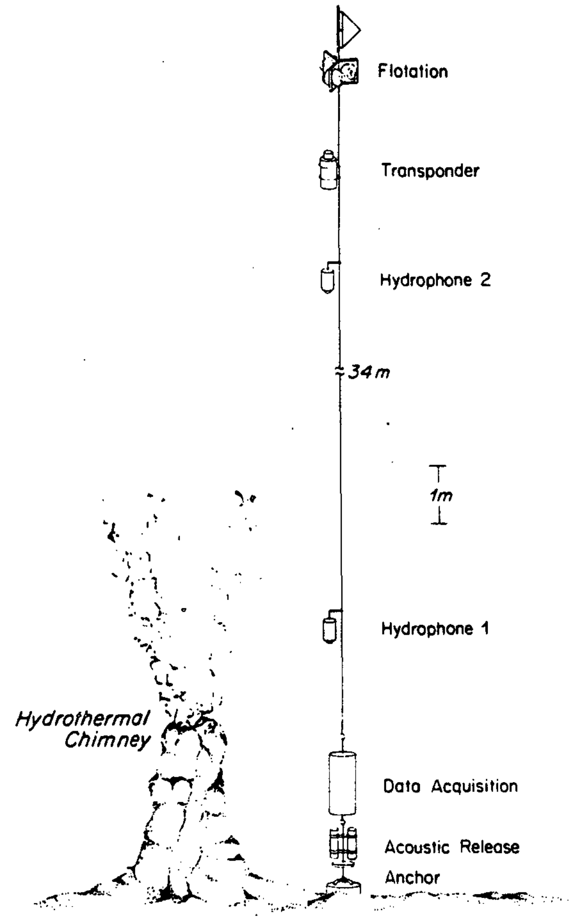

Fig. 4. Detail of instrumented cable and deployment scheme. Lower hydrophone was 2-3 m from vent orifice; upper hydrophone was 38-40 m above lower.

ocean. Due to the fact that all the sources of fluctuations are not completely known, only a statistical description is permitted, based on observations over an extended time period. In producing our statistical description of the hydrophone output and in analyzing the sound we will use several assumptions. First, we will assume that the noise is temporally stationary over our individual sample periods. This enables interpretation of Fourier transforms of the time series as representative of the distribution of power over frequency. To help validate this assumption, examinations of the time series will be used to eliminate impulsive signals and gross differences with time. The second assumption is that the signal from the vent is constant over the duration of the experiment. Visual observations of the smokers support this assumption as the flow velocity appeared to remain constant from dive to dive.

Power spectra are calculated for this analysis using the Welsh method [*Oppenheim and Schafer*, 1975]. The 8192-point records were divided into 16 sets of 512 points, each set multiplied by a Hanning window, and used with a fast Fourier transform (FFT) algorithm to compute the power spectral densities which are subsequently averaged together. This gives a power estimation accuracy of $P/\sqrt{N} = P/4$, where N is the number of sets and P is the power level at a given frequency. The frequency resolution of $1/T$, where T is the time length of a set, is 0.6 Hz for the 300-Hz samples and 4.7 Hz for the 2400-Hz samples.

In addition to comparisons of simple power spectra, the coherence and phase between the two channels will be examined. The coherence level reveals the amount of signal common to both receivers, while the phase differences at a given frequency provide information on the angle of incidence of the incoming wave. The direction of wave travel can be obtained by looking at linear trends in phase as a function of frequency. Phase is calculated here such that if a broadband signal impinges on the array at an angle θ from above, the phase will be a linearly increasing trend in frequency whose slope is dependent on θ and receiver separation. If the waves arrive from below, phase will decrease with increasing frequency.

ANALYSIS OF NOISE FIELD

Two power spectra encompassing bandwidths of 1-800 Hz from the first deployment (Inferno) and 1-100 Hz for the second (Hell), presented in Figures 5 and 6, represent two of the lower-noise periods of the experiment. The most obvious feature in these spectra is the difference in power levels between the two hydrophones in the bandwidth 10-200 Hz, with the upper hydrophone receiving more power than the lower. Further, a comparison with ambient ocean noise curves (Figure 1, from *Urick* [1986]) reveals a marked similarity in power levels and spectral shape. We hypothesize that most of the noise recorded in the caldera is due to the ambient ocean noise sources described above and that the major difference in signal level is due to a shadowing and reflecting effect by the nearby caldera wall. The following analysis examines this hypothesis in detail.

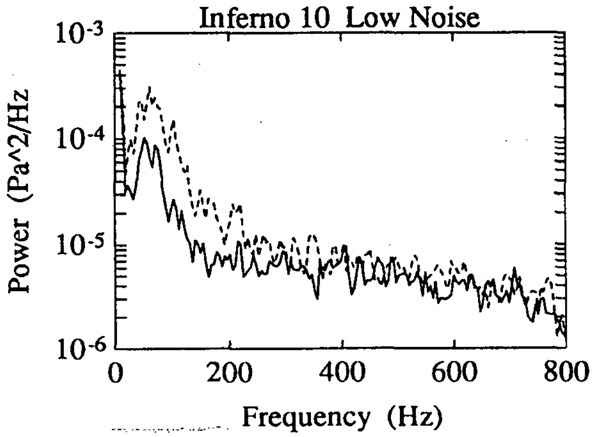

Fig. 5. Low noise period power spectral density from Inferno deployment (record 10) of bandwidth 1-800 Hz. Solid curve is for lower hydrophone (close to the vent), and dashed curve is for upper hydrophone. Differences in the bandwidth 30-250 Hz are attributed to effects of the caldera wall on ambient ocean noise.

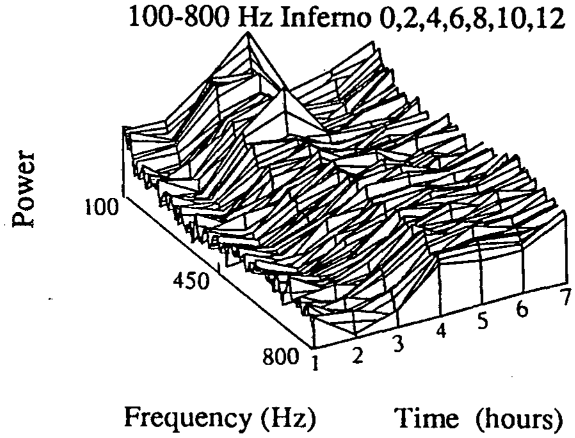

Fig. 7. Hourly time history of spectra from Inferno deployment (lower hydrophone) of bandwidth 100-800 Hz showing increasing energy toward end of deployment which corresponds to increasing wind velocity.

High-Frequency Band: 100-800 Hz

Sound in this frequency band is dominated by sea state and wind force and will experience changes on a time scale of several hours to days. An examination of the time history for the Inferno deployment (Figure 7) reveals power variations of about a factor of 3 for the bandwidth 200-800 Hz over the course of the deployment. The ship's log records a constant sea state of 1 to 2 m and wind increasing from 18 to 38 km/h over the deployment. This is consistent with the general trend of increasing power seen in Figure 7.

Weather-related sound propagates downward from the sea surface with sea conditions directly overhead exerting the most influence on sound at the seafloor below. Since sound waves are travelling to the receiver array from above, one would expect little or no caldera wall effects on this bandwidth if the sources are indeed weather related. Figure 8 supports this as there is very little difference in power between the two receivers above about 250 Hz. Although the coherence is generally weak (Figure 9), it is to be expected for wavelengths short as compared to receiver separation. A look at the cross correlation reveals the highest correlation for a lag (0.0267 s) corresponding to an end-on wave approach from above (Figure 10), suggesting sources at the sea surface.

Medium-Frequency Band: 5-100 Hz

Sound from distant shipping, travelling horizontally large distances (hundreds to thousands of kilometers), often in the sound channel, will depend on both traffic density and speed and propagation path characteristics. Time variations are expected to be of the order of hours but may be punctuated by local sources such as ships overhead (Figures 11*a* and 11*b*). It is because these waves from distant sources travel very close to horizontal that the caldera wall can influence the sound at the vent field. All the sound arriving from the west must diffract around the edge of the wall to reach the lower receiver as it is in the geometric shadow of eastward travelling acoustic waves (Figure 3). In addition, westward travelling waves can reflect off the wall and increase the power levels at the upper receiver, while the lower receiver,

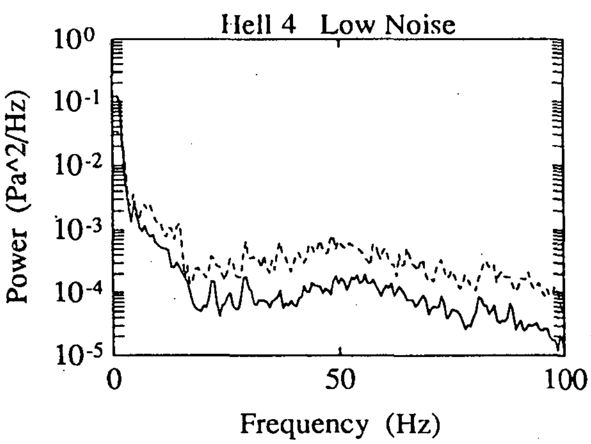

Fig. 6. Low noise period power spectral density from Hell deployment (record 4) of bandwidth 1-100 Hz. Solid curve is for lower hydrophone (close to vent), and dashed curve is for upper hydrophone. This details differences in sound level caused by the wall in the bandwidth 0.5-100 Hz.

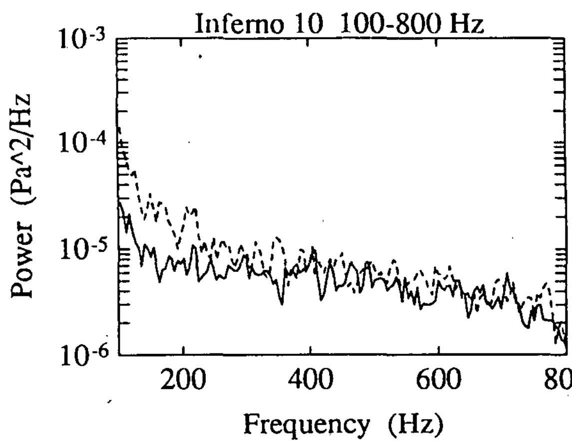

Fig. 8. Low noise period power spectral density from Inferno deployment (record 10) showing difference in upper (dashed curve) and lower (solid curve) hydrophone power levels out to 250 Hz, followed by similar levels to 800 Hz. This due to the caldera wall affecting horizontally travelling 20-250 Hz waves and not influencing 250-800 Hz vertically travelling waves.

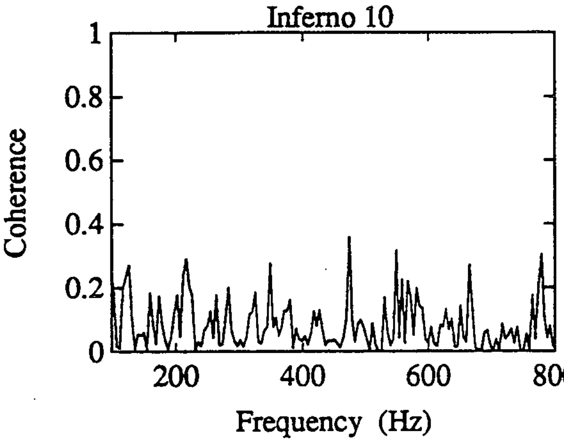

Fig. 9. Coherence between upper and lower hydrophones for bandwidth 100-800 Hz for Inferno (record 10).

being so close to the bottom, will intercept fewer reflected waves. Several effects are seen in the power spectra which support this hypothesis. First, the upper hydrophone has up to 4 times as much power in the affected bandwidth as the lower (Figures 12*a*, 12*b*, and 12*c*). Second, the effect should drop off at low frequencies as the wavelength of sound approaches the dimensions of the wall. Wavelengths near 75 m and longer, 20 Hz and below, will be less influenced by the wall and hence reach both receivers more equally, as can be seen in Figures 12*a* and 12*b*. Power differences should also be reduced at higher frequencies, above 200 Hz, because the predominant sound at these frequencies is not travelling horizontally, as was seen above (Figure 12*c*). Third, the second deployment should show slightly greater differences since Hell vent is 15 m closer to the caldera wall than Inferno; this is seen in Figures 12*a* and 12*b*. Finally, the phase difference of the waves at the two receivers should be roughly zero and constant as the sound hits the array broadside from westward travelling waves. Figures 13*a*, 13*b*, and 13*c* present power, coherence, and phase for a record taken during Hell (record 8) deployment. The generally low coherence is expected if one receiver samples part of a sound field not sampled by the other. However, the coherence is markedly above random, and the phase significant as can be seen

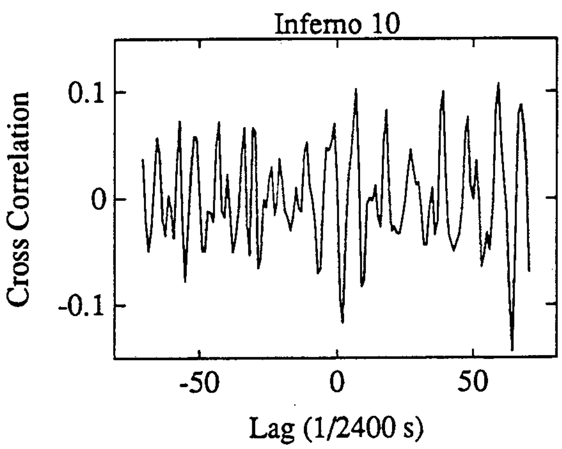

Fig. 10. Cross correlation between upper and lower hydrophone for high-pass-filtered (above 200 Hz) Inferno low noise period (record 10). Greatest magnitude of correlation occurs at a lag of 64 points, which corresponds to the receiver separation, implying that the waves are impinging on the array from end-on (from above).

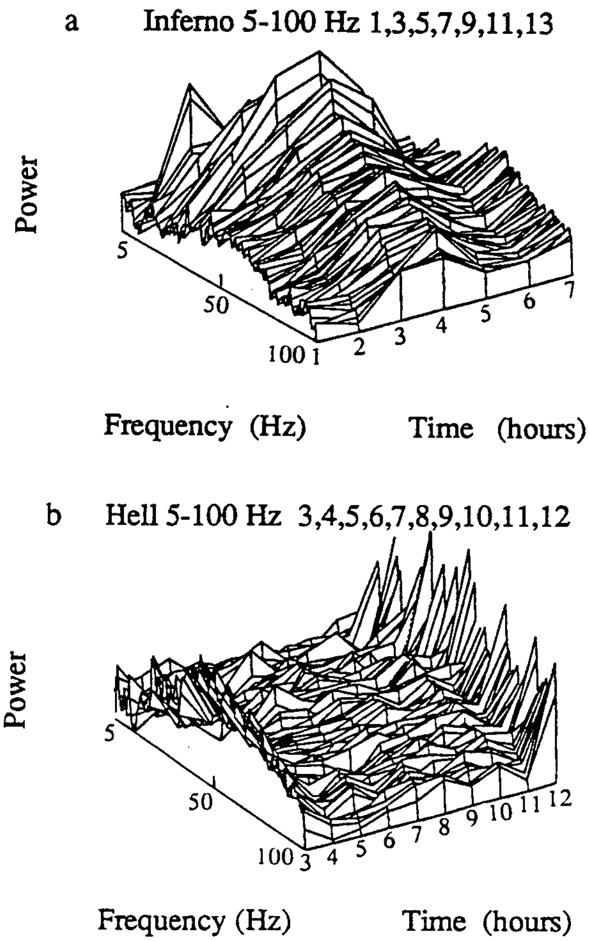

Fig. 11. (*a*) Hourly time history of spectra from Inferno deployment for bandwidth 5-100 Hz, showing a general increase during the middle of the deployment, probably in response to an increase in ship activity. (*b*) Hourly time history of spectra from Hell deployment for bandwidth 5-100 Hz, showing relatively constant levels except for the first and last hour during which time *Atlantis II* was in close proximity to the vent site.

by comparing them to coherence and phase calculated between two totally uncorrelated samples taken hours apart (Figure 14). The phase between 20 and 100 Hz on Hell 8 is quite constant and near zero (compare to uncorrelated phases in Figures 14*a* and 14*b*), implying that the sound impinges at right angles to the vertical array and is thus travelling horizontally.

Low-Frequency Band: 0.25-10 Hz

There appear to be two major types of sound in this band, one microseisms caused by local sea surface waves, and the other of unknown origin which produces evanescent interface waves travelling along the seafloor boundary whose amplitudes decay exponentially with distance from the boundary [*Dowling and Ffowcs Williams*, 1983].

Microseism power changes slowly since it is tied to changing sea state. The interface waves apparently change amplitude abruptly, as seen in the time series from Hell record 8 in Figure 15, where microseisms are followed by interface waves arriving at t=22 s. The upper hydrophone, being less influenced by interface waves, should have slower and lower amplitude variability than the lower hydrophone. Figures 15-18 depict this effect and show the striking difference between microseism and interface waveforms. A record from Inferno (record 1) (Figure 16) and one from

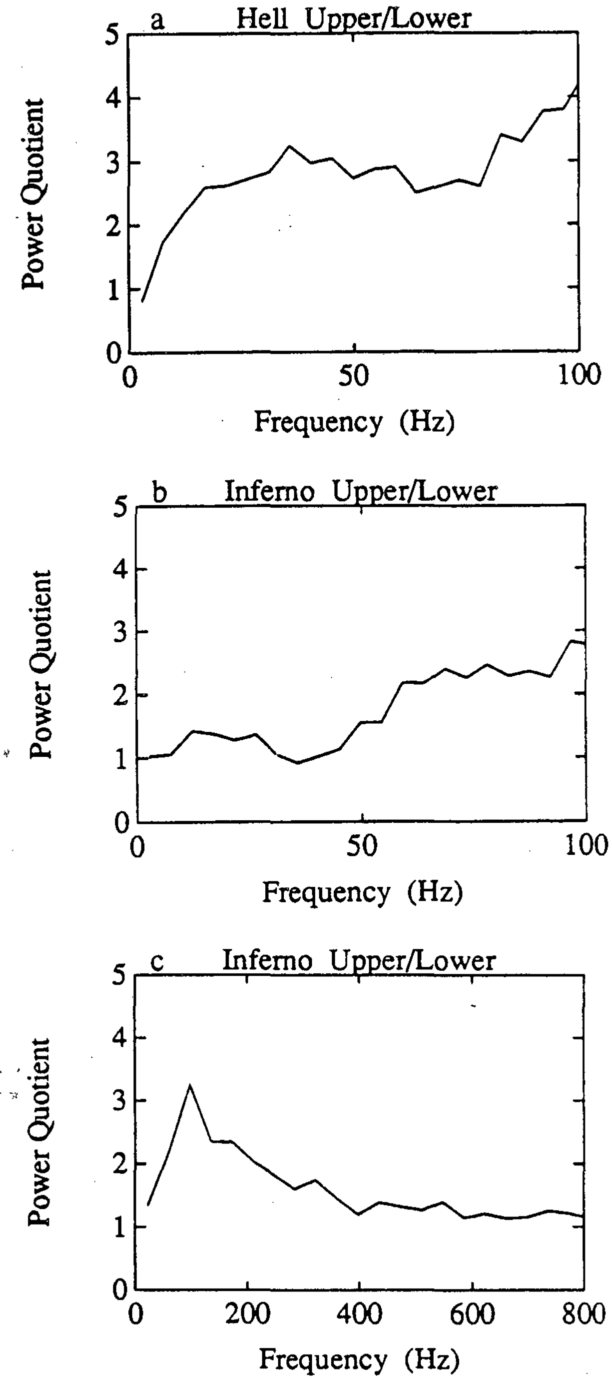

Fig. 12. Ratios of upper and lower hydrophone power levels for all records from (*a*) Hell deployment, (*b*) Inferno deployment: 1-100 Hz and, (*c*) Inferno deployment: 1-800 Hz. Notice that the quotient decreases with both decreasing and increasing frequency, centered around typical distant shipping frequencies of 30-200 Hz. This difference is due to effects of the caldera wall.

Hell (record 9) (Figure 17) show nearly identical low-frequency waves, in phase, as expected from long-wavelength microseisms. The second record from Hell (record 5) (Figure 18), taken 4 hours earlier, shows high-amplitude interface waves on the lower hydrophone and typical microseismic amplitude waves on the upper, exemplifying the effect that interface wave amplitude dies away rapidly from the seafloor. The power, coherence and phase confirm the conclusions of the visual examination of the time series (Figurea 19*a*, 19*b*, and 19*c*). In Figures 19*b* and 19*c* the high coherence and constant phase for microseisms can be seen. In Figures 20*b* and 20*c* are shown the low coherence and variabie phase for the interface waves.

The very rapid drop in pressure away from the interface is most pronounced for the frequency band 0.5-3 Hz, shown in the power spectra (Figure 21*a*) and amplitude ratio (Figure 21*b*) from Hell record 5. It is difficult to produce such a drop in amplitude at low

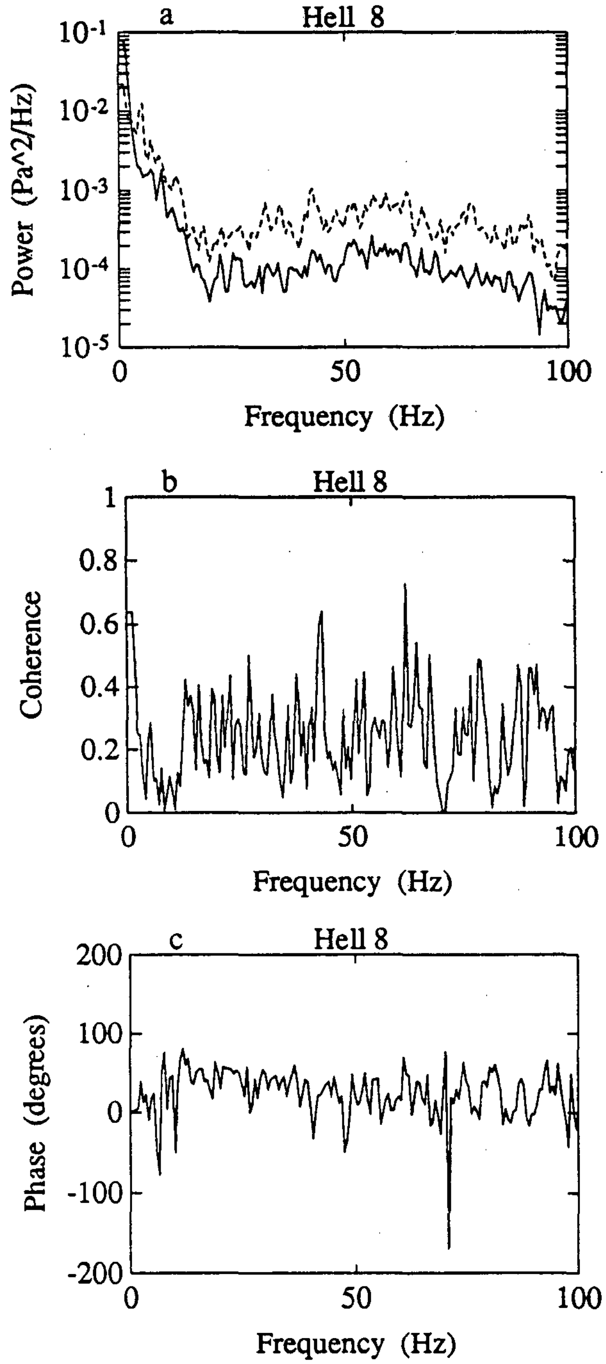

Fig. 13. (*a*) Power spectral density for low noise period of Hell deployment (record 8). Solid curve is lower hydrophone; dashed curve is upper hydrophone. (*b*) Coherence between upper and lower hydrophones for low noise period of Hell deployment (record 8). Coherence, although low, is significant (compare to Figure 14). (*c*) Phase for same period showing relatively constant and zero phase produced by waves impinging on the array broadside because they were travelling horizontally.

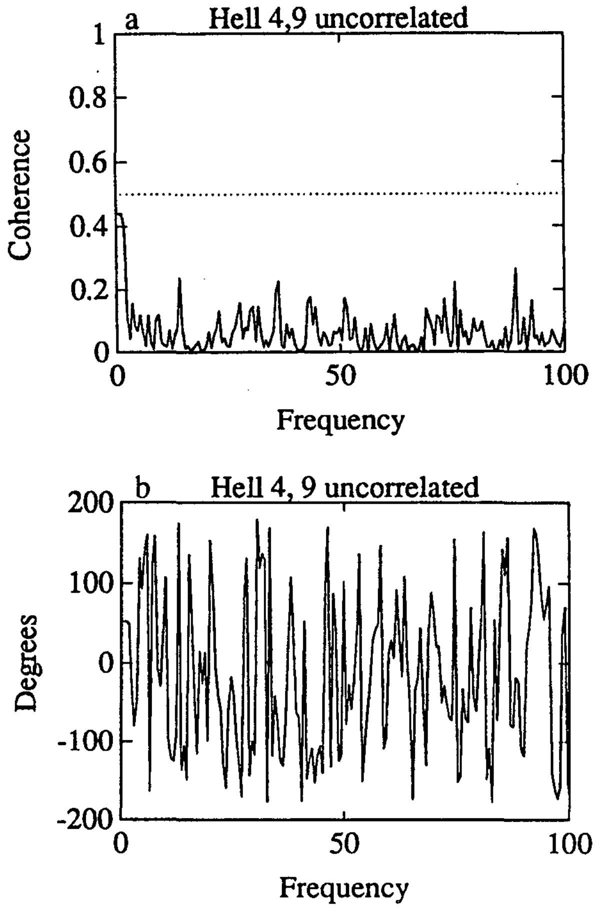

Fig. 14. (*a*) Coherence calculated between records taken from upper and lower hydrophones at two different times (totally uncorrelated). Note the low level of this random coherence. (*b*) Phase for same records. Note the completely random phase (especially as compared to Figure 13*b*).

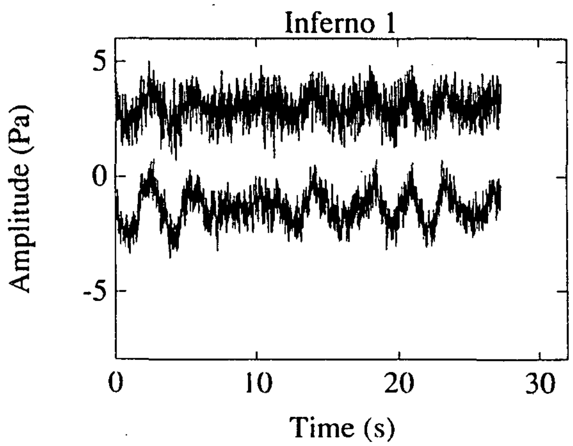

Fig. 16. Time series pressure level from Inferno deployment (record 1); upper trace is from upper hydrophone and vice versa. Note similarity in phase and pressure level for low-frequency oscillations on both hydrophones due to microseisms.

frequencies except with slow moving evanescent waves such as Stoneley waves. Stoneley waves are interface waves which can exist between a solid and a liquid and whose amplitudes die away exponentially in the liquid layer. They can be produced by spherical wave fronts, and generally, the source must be within one wavelength of the interface. If we assume that these are Stoneley waves, then we can calculate the Stoneley wave velocity with the equation for Stoneley wave amplitude (equation (1) [*Dowling and Ffowcs Williams*, 1983]) and using the amplitude ratio between the upper and lower hydrophone as a funtion of frequency.

$$P = Ae^{i\omega(t-px)-\gamma z} \tag{1}$$

where p is the ray parameter, x is horizontal distance, z is vertical distance, and

$$\gamma = \omega\sqrt{\frac{1}{\alpha_s^2} - \frac{1}{\alpha_w^2}} \tag{2}$$

This leads to an equation for α_s of the form

$$\alpha_s = \sqrt{\frac{1}{\left(\frac{ln \frac{P_1}{P_2}}{\omega z_d}\right)^2 + \frac{1}{\alpha_w^2}}} \tag{3}$$

where α_s is the Stoneley wave velocity, α_w is the p-wave velocity in water, P_1 is the pressure at the lower hydrophone, P_2 is the pressure at the upper hydrophone, ω is the angular frequency, and z_d is the distance between the two hydrophones. We use z_d = 0.039 km and α_w = 1.485 km/s (from concurrent conductivity, temperature, and depth (CTD) measurements made in Axial Volcano).

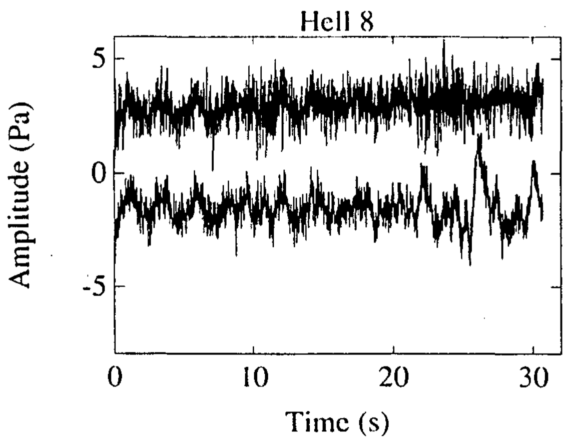

Fig. 15. Time series pressure level from Hell deployment (record 8); upper trace is from upper hydrophone and vice versa (traces have been offset around zero for display). Traces are similar until time t=22 s when interface waves begin to dominate the lower signal.

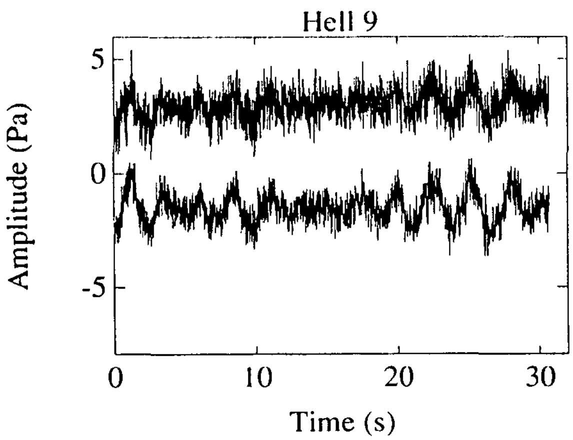

Fig. 17. Time series pressure level from Hell deployment (record 9); upper trace is from upper hydrophone and vice versa. Note similarity in phase and pressure level for low-frequency oscillations on both hydrophones due to microseisms.

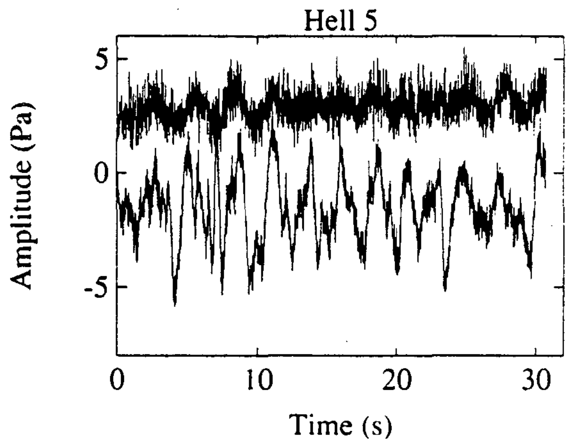

Fig. 18. Time series pressure level from Hell deployment (record 5); upper trace is from upper hydrophone and vice versa. Note large-amplitude erratic oscillations on lower hydrophone not seen on upper hydrophone. Upper hydrophone shows typical microseism oscillations while lower records passage of interface waves which poorly penetrate water column.

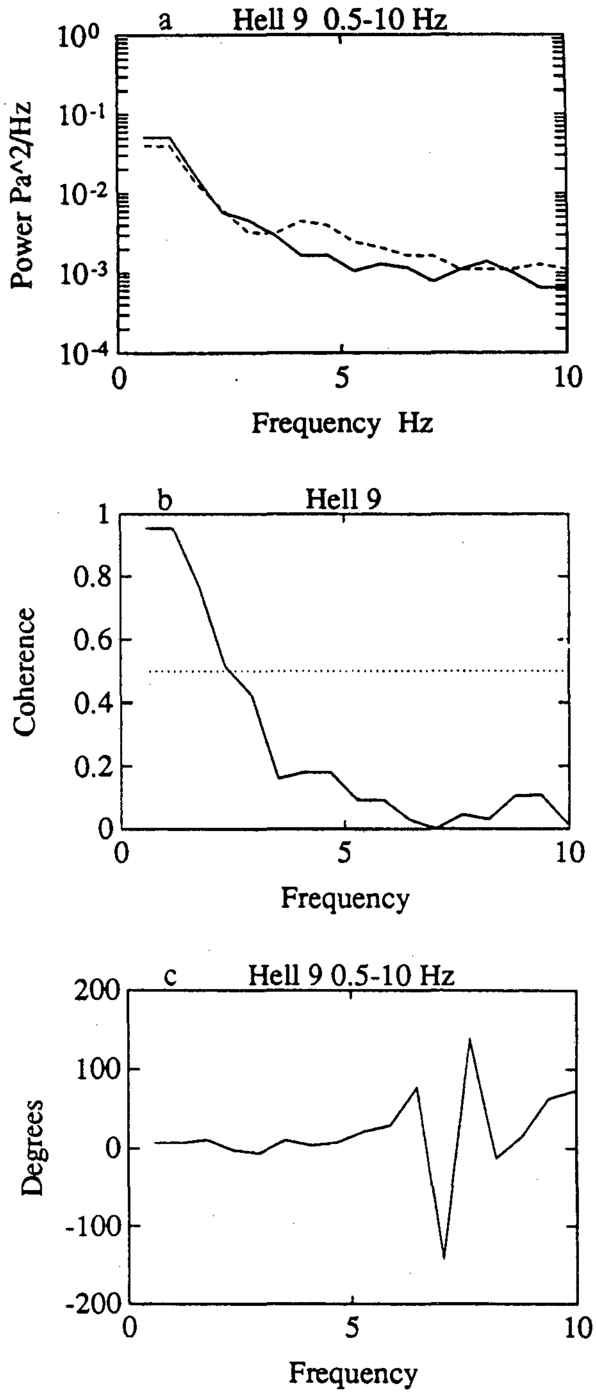

Fig. 19. (*a*) Upper part shows power levels from Hell (record 9) in 0.5-10 Hz bandwidth. Note similarity in power between upper hydrophone (dashed curve) and lower hydrophone (solid curve) due to microseism energy. (*b*) Lower part shows high coherence between the two hydrophones from 0.5 to 3 Hz characteristic of microseisms. (*c*) This shows the constant and zero phase between upper and lower hydrophone.

Using equation (3) and the amplitude ratio from Figure 21*b* produces α_s as a function of frequency (Figure 22). Further, with $\lambda = \alpha_s/f$, λ as a function of frequency can be plotted (Figure 23). If the source must be within one wavelength of the interface, then for frequencies between 0.5 and 3 Hz, it must be less than 500 m away, and probably about 100 m from the interface (either in the water column or seafloor).

Stoneley waves are theoretically nondispersive in a homogeneous, infinte, halfspace, that is, α_s should be independent of frequency. Allowing for errors due to finite time series length and dispersion due crustal inhomogeneities, an estimate of α_s for frequencies between 0.5 and 3 Hz is $\alpha_s = 0.1$ km/s, obtained from Figure 22. Theoretically, α_s is just slightly less (about 98%) than α_w if $\alpha_w < \beta_2$ (where β_2 is the shear wave velocity in the crust), and slightly less than β_2 if $\beta_2 < \alpha_w$. With $\alpha_w = 1.485$ km/s, the conclusion is that β_2 is approximately 0.1 km/s, or very slow. This implies that the solid medium is composed of a very unconsolidated material and that the source is local. The source could well be moving magma or large-scale, subsurface, hydrothermal fluid motion.

In summary, the general power spectral level, time variability, power differences, and wave phase relationships suggest that the bulk of recorded sound is attributable to the identifiable ocean noise sources of microseisms, distant shipping, and ocean surface weather. However, several records present striking evidence of evanescent interface waves, generated perhaps by large local events such as magma or fluid movement.

Isolated Events

Several individual noise events were recorded during the course of this experiment. One record taken during Inferno deployment (record 3) captured a monochromatic 19-Hz sound signal which we attribute to a whale (Figure 24). The signal has high power (Figure 25*a*), coherence (Figure 25*b*), and the phase shows that the signal is coming in end-on from above (Figure 25*c*). The separation d of the receivers is such that for this frequency, $d = 1/2\lambda$, so sound arriving from above will have a phase delay between the two receivers of $180°$, as is seen in Figure 25*c*. Curiously, the amplitude is higher on the lower hydrophone than on the upper, due perhaps to some focussing effect of the topography causing constructive interference on the lower and destructive on the upper.

Similar power and phase phenomena are seen on a record taken when *Atlantis II* is the sound source. Figure 26*a* shows the power spectra of noise with the ship overhead and slightly eastward of the vent site. There is very high coherence in the signals (Figure 26*b*) and a linear phase with slope describing waves coming in end-on (Figure 26*c*). At 20 Hz the $180°$ phase shift is evident, similar to that of the whale.

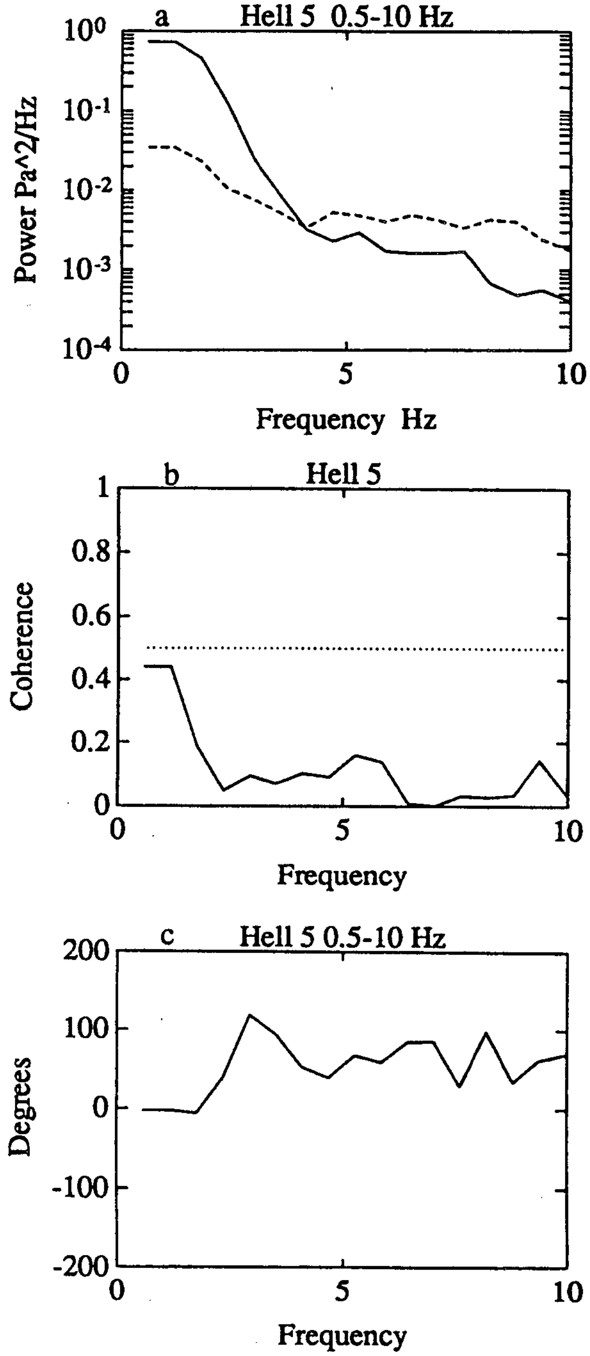

Fig. 20. (*a*) Upper part shows high power level on lower hydrophone (solid curve) and lower power on upper hydrophone (dashed curve) for Hell deployment (record 5). (*b*) Low coherence between the two hydrophones is seen since pressure levels at lower hydrophone are due to interface waves not seen on upper hydrophone. (*c*) This shows nonconstant and nonzero phase as is expected between the upper and lower hydrophones since they are receiving different signals.

Hydrothermal Noise Detection

Neither Hell nor Inferno vents produce enough sound to isolate unambiguously their entire spectrum levels from ambient ocean noise. In fact, as seen above, overall noise levels are higher far from the vents than they are close to them. This unexpected result makes direct comparisons of simultaneous but spatially separated noise spectra difficult. In order to identify regions of the spectra which may have vent signal, we must identify a background

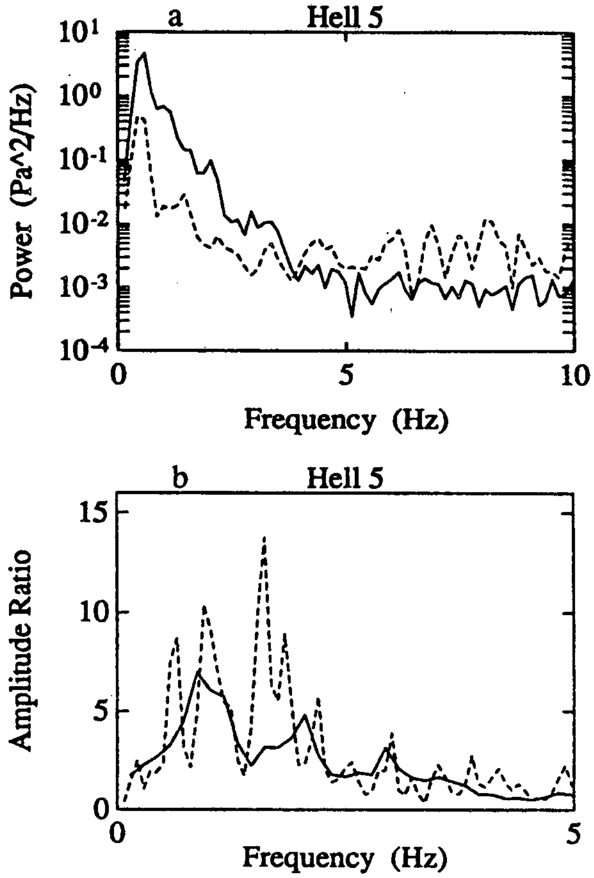

Fig. 21. (*a*) Power spectra from Hell (record 5), with a 2048-point FFT (solid curve is from lower hydrophone, dashed curve is from upper hydrophone), showing difference in power at frequencies between 0.5 and 3 Hz due to interface waves picked up on the lower hydrophone. (*b*) Ratio of pressure amplitudes (lower hydrophone/upper hydrophone) from Hell (record 5) for 2048-point FFT (lower-amplitude curve) and 4096-point FFT (higher amplitudes).

noise level for this site. It had been hoped that the far receiver would provide this information, but geometrical influences, i.e., the caldera wall, proved to be too significant and complex. As an alternative, we have chosen to represent background ambient ocean noise with the lowest recorded noise spectra. Anything

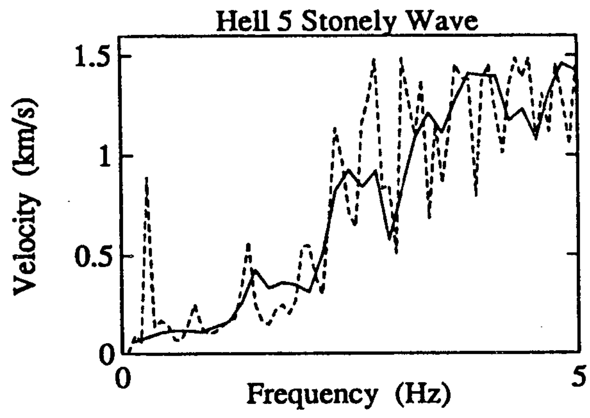

Fig. 22. Stoneley wave velocity calculated using amplitude ratios in Figure 21*b* (the curve from the 2048-point FFT is smoother and has higher amplitude than that from the 4096-point FFT).

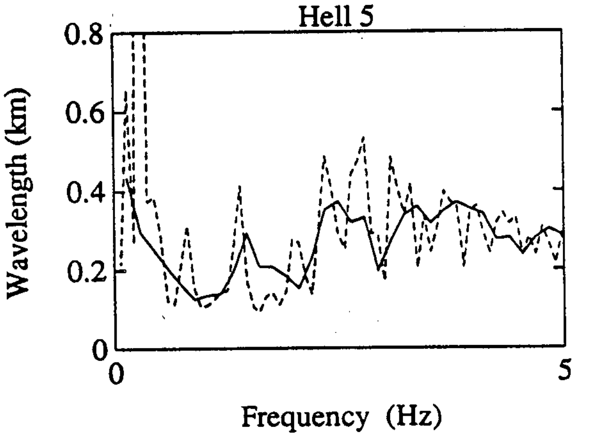

Fig. 23. Wavelength calculated from the Stoneley wave velocity in Figure 22. Dashed curve is from the 4096-point FFT; solid curve is from the 2048-point FFT.

recorded significantly above this, as defined below, will be considered a signal which we will attempt to attribute to known sources.

Since all analyses are within a statistical framework, it is useful to assign significance by examining the probability that a given signal is real and not a chance fluctuation. The effective signal to noise level will be described here using a value called the detection index [*Burdick*, 1984; *Bangs and Schultheiss*, 1973; *Owsley and Swope*, 1981]. This is an array output signal-to-noise ratio which depends on the number of receivers, the sample length, and the signal field and noise field. It describes both the probability of detection and the probability of false alarm (mistakenly detecting a signal when its not present) for a given signal and noise input to the hydrophones (see Appendix B). A high detection index provides simultaneously high confidence in correctly detecting a signal when it is present and in not falsely detecting one when it is absent. We will calculate this detection index by assigning the lowest power level record to be noise, comparing the other records to these values and designating as signal anything above the noise. The magnitude of the resulting detection indices will represent our confidence in a given signal. We will deem as significant any detection index over 10, a value which represents a probability of detection of 90% and probability of false alarm of 5%.

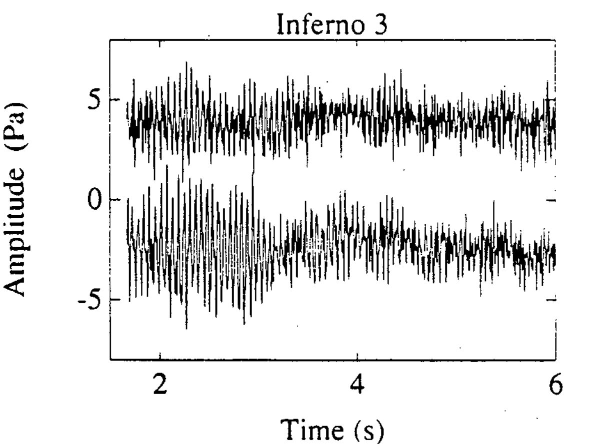

Fig. 24. Upper trace is pressure level from upper hydrophone; lower trace is pressure level at lower hydrophone. The beginning of this period from Inferno (record 3) a monochromatic 19-Hz signal is detected, which we attribute to a whale.

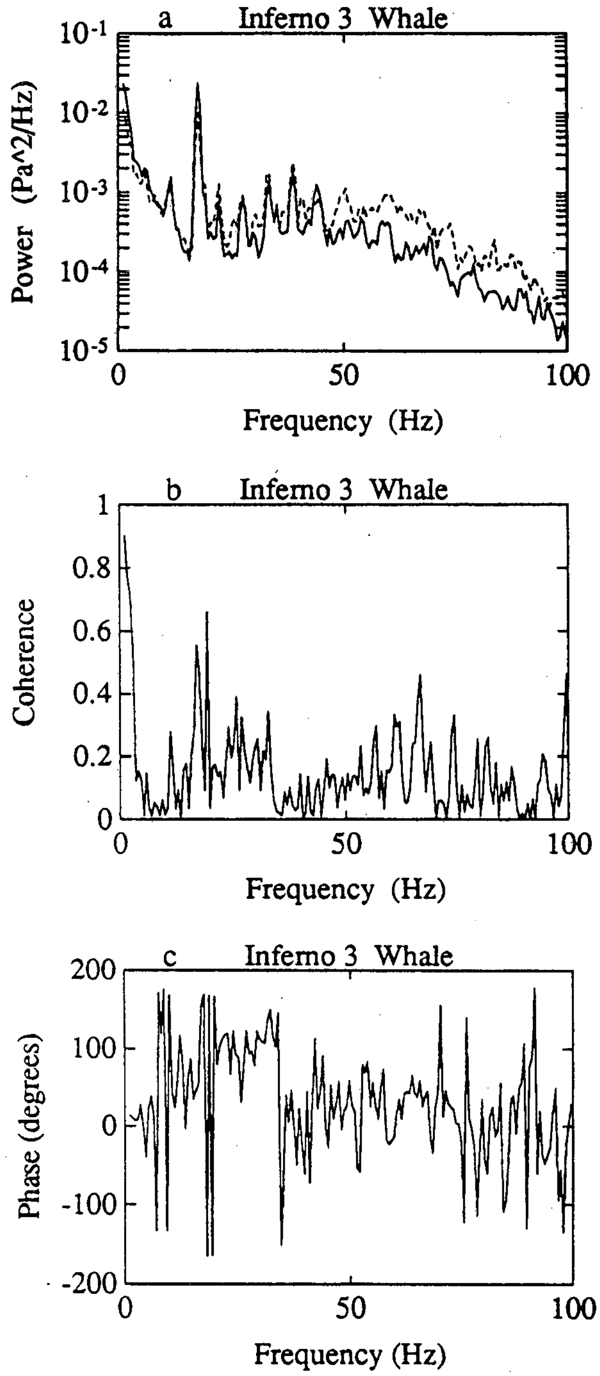

Fig. 25. (*a*) Power spectral density for Inferno (record 3), solid curve is from lower hydrophone, dashed curve is from upper hydrophone, showing peak at 19 Hz attributed to a whale. The amplitude is higher on lower hydrophone due to reflections causing constructive interference on the lower phone and destructive on the upper. (*b*) Coherence between upper hydrophone and lower for Inferno (record 3) which detected 19-Hz signal. (*c*) Phase between upper and lower hydrophone (Inferno record 3) showing 180° phase shift near 20 Hz. This is due to the fact that the receiver separation is approximately twice the wavelength at this frequency, and hence waves coming into the array end-on will see a 180° phase delay between the two receivers.

The average of the lowest noise spectra, one set from Hell and the other from Inferno, assigned to represent ambient ocean noise (Figure 27), are remarkably similar considering they were recorded several days apart. The lower hydrophone near Hell will be used for comparison to Inferno and vice versa, based on the

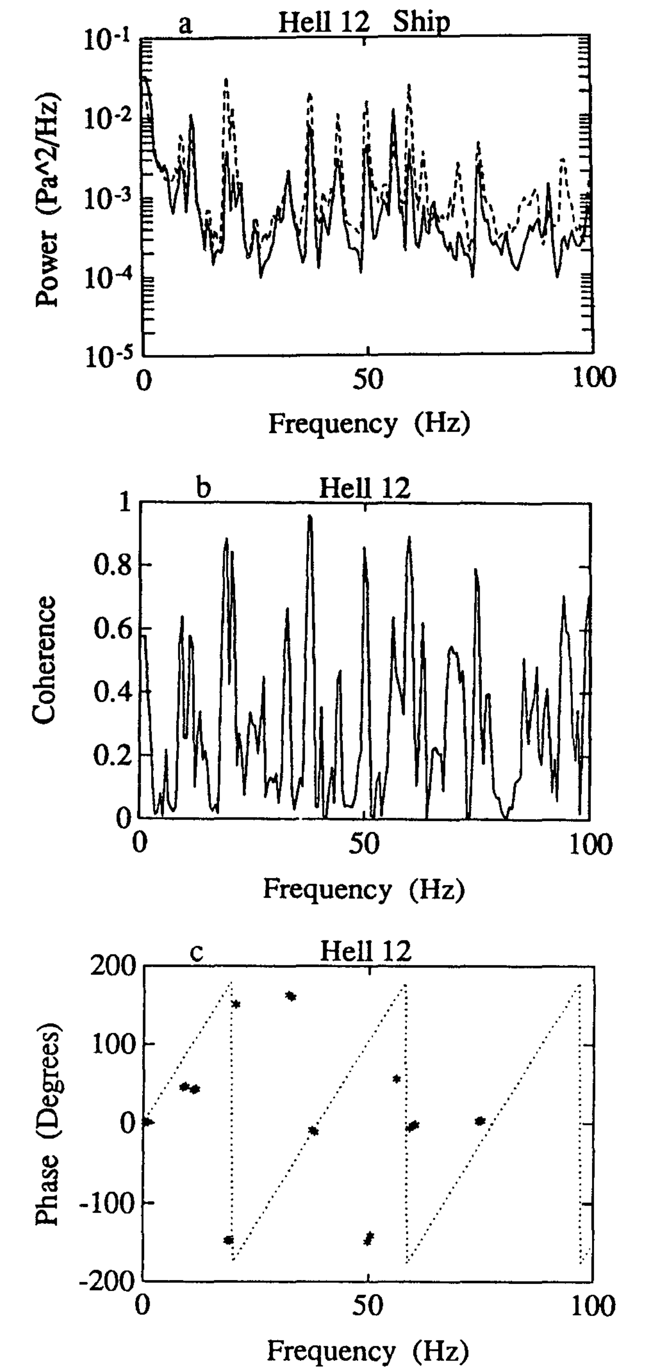

Fig. 26. (*a*) Power spectral density from Hell deployment (record 12) when *Atlantis II* is overhead and slightly northeast of the vent site. Peaks and harmonics are typical of near-ship noise. (*b*) Coherence between two receivers for Hell (12) when ship is near. Notice extremely high coherence at ship's frequencies. (*c*) Transfer phase between the two receivers for this record. Linear trend from 1 to 20 Hz implies waves are arriving from nearly vertical.

logic that the vents are not exactly identical and any differences in sound level due to venting should be apparent given the 35-m separation between vents.

When we compare the quietest record at Hell with background Inferno noise we find that the detection indices at all frequencies are less than 10, as shown in Figure 28*a*. Also, when the quietest record from Inferno is compared to background at Hell, the indices are all less than 10 (Figure 28*b*). We must conclude that the sound produced by the vents are below the 90% confidence detection limit of this array in this noise field, a detection limit that is equivalent to a signal-to-noise ratio (SNR) of about 10 in a 5-Hz band, or about 10^{-4} Pa^2/Hz.

We will note here, however, that Inferno appears to be generating a small sound signal at about 40 Hz, as seen in Figure 27, of approximately 1×10^{-4} Pa^2/Hz. This signal is evident on the two lowest-noise 300-Hz bandwidth records. The other five contain high noise on both channels at this frequency as well as others, probably due to an undocumented ship or submarine in the area, and no conclusions can be drawn from these. The frequency and power level of Inferno vent are consistent with theoretical estimates of noise from a jet (see Appendix A). A velocity of 2 m/s from the 0.04-m orifice would generate sound with a peak frequency of 40 Hz. Sound pressure level at 2.3 m in the near field region of a cold turbulent jet is predicted to be 2×10^{-4} Pa at peak frequency (a power level of about 4×10^{-8} Pa^2/Hz). A hot, 350°C jet exiting into cold seawater can produce up to a factor of 10^6 higher power levels, through the amplification of sound by convecting flow inhomogeneities [*Morfey, 1973*]. The data from the Inferno deployment show a factor of about 10^3 elevation in power levels over expected cold jet sound, which we attribute to the high temperature and consequently low density of the exiting hydrothermal fluid. The lack of higher signal levels indicates that monopole and dipole sound sources are not present at this vent site (see Appendix A).

Comparison with other Hydrothermal Noise Measurements

East Pacific Rise. The first indication of vent sound generation came from data collected near hydrothermal vents at 21°N on the East Pacific Rise (EPR) where an array of ocean bottom hydrophones was set out to study microearthquake activity at an active vent site [*Riedesel et al.*, 1982]. In comparing two hydrophones, located 300 m and 2 km from the vents, it was noted that the automatic gain control on the instrument nearer the vents set itself to a gain level 16-64 times less sensitive than that of the instrument far away. This indicated that the intensity of ambient sound near the vent was consistently louder than the sound farther away, suggesting that the major source of ambient noise in this area was the hydrothermal vents [*Riedesel et al.*, 1982].

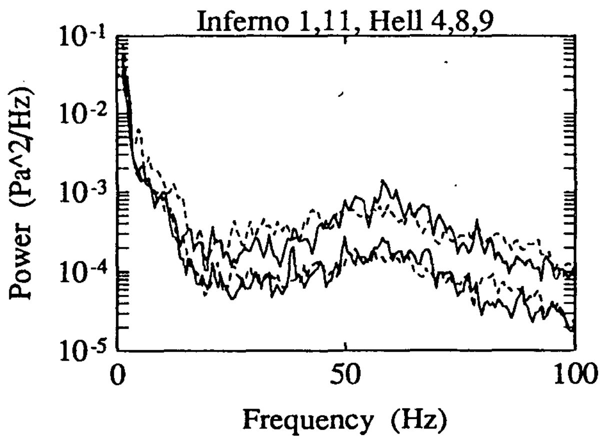

Fig. 27. Low noise records used for calculation of signal detection index, average of Inferno records 1 and 11 (upper solid curve from upper hydrophone, lower solid curve from lower hydrophone) and Hell records 4, 8, and 9 (upper dashed curve from upper hydrophone, lower dashed curve from lower hydrophone). Note small peak in lower Inferno power spectral density near 38 Hz; this is attributed to jet noise from Inferno vent.

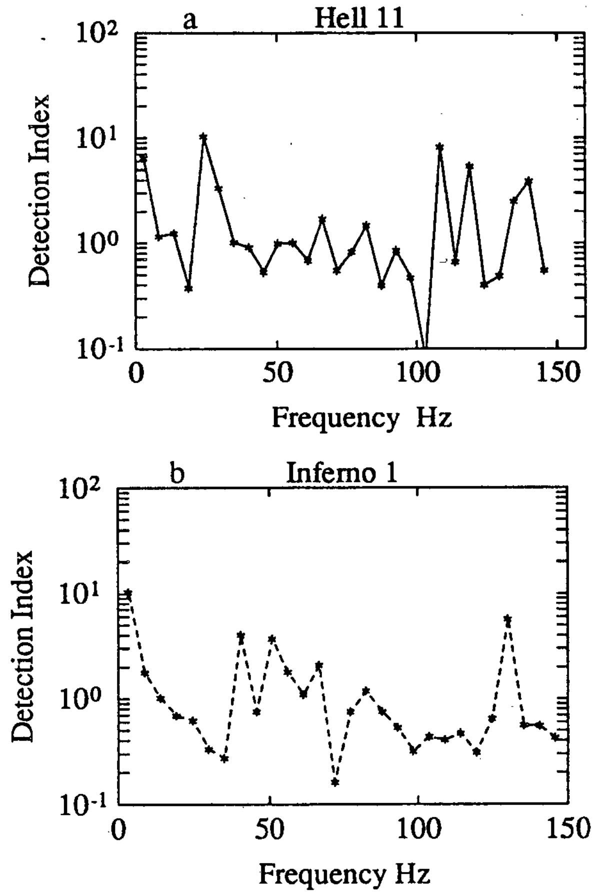

Fig. 28. (*a*) Signal detection index for low noise Hell deployment (record 11); note that nowhere is the signal-to-noise ratio (SNR) greater than 10, the value which corresponds to a 90% confidence in signal detection with a 5% false alarm rate. (*b*) Detection index for low noise Inferno deployment (record 1), note that nowhere is the SNR greater than 10, the value which corresponds to a 90% confidence in signal detection with a 5% false alarm rate.

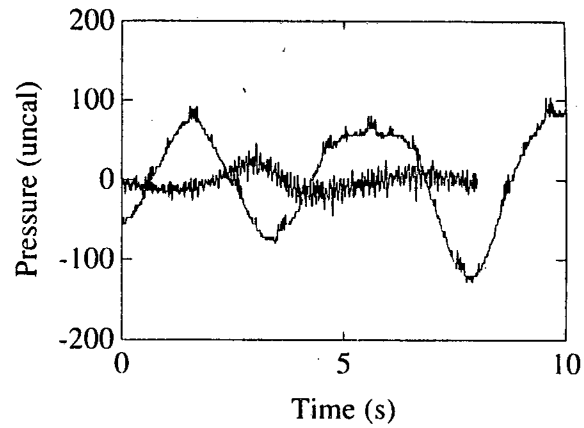

Fig. 29. Time series of data from two hydrophones near 21° N on the EPR. Larger-amplitude, low-frequency record is from the hydrophone 300 m from the vents and the other from the hydrophone 2 km away.

An inspection of a time series record (Figure 29) reveals a major difference in amplitude at very low frequencies (0.16 Hz). These frequencies are usually associated with surface-generated microseisms [*Webb*, 1984], but it is not clear why the amplitude should be so different at a receiver separation of only 1.5 km. These data are suggestive of a low-frequency sound source located near the vents, but the evidence is inconclusive.

Juan de Fuca Ridge. Anomalous high ambient acoustic noise was observed in the caldera of Axial Seamount at 46° N on the Juan de Fuca Ridge [*Bibee and Jacobson*, 1986]. Noise levels from 2 to 30 Hz varied up to 25 dB over 6 km as measured on four separate receivers, and it was suggested that the noise source was at or near the seafloor. With the assumption of spherical spreading, the source was placed at 400 m from one of the instruments, in the northern part of the caldera. This placed it within 200 m of a low-temperature vent field mapped on a previous expedition [*Chase et al.*, 1983]. However, an instrument placed several hundred meters from the known high-temperature vent field Ashes, located in the southwestern part of the caldera, recorded no evidence of anomalous acoustic noise.

Argo and towed hydrophone. In December 1985, we attached a deep-sea hydrophone to the Argo televiewer and geophysical instrument sled during the survey of the East Pacific Rise (EPR) between latitudes 10° and 12° N [*Argo-Rise Group*, 1988]. Noise was recorded in real time on the ship via Argo's conducting cable. Digital samples were taken at 1000 Hz every hour and when in the vicinity of hydrothermal areas. The vehicle was passively towed by the surface ship, and flow noise was minimized by reducing the Argo's horizontal velocity to less than 0.4 km/h. Unfortunately, a heave compensator was not able to remove all the vertical motions induced by the surface swell; thus, only about 10% of the recorded data was uncontaminated by vertical flow noise. Few vigorous black smokers were encountered during the 200+ hours of slaloming down the ridge crest, but five hydrothermally active areas, as defined by biota, were crossed. Comparison of sound recordings near (within several meters) and far (farther than 1000 m) from these areas revealed consistently elevated sound levels near hydrothermal sites (Figures 30*a*, 30*b*, 30*c*, and 30*d*) at frequencies generally between 15 and 30 Hz. Unfortunately, absolute power levels were unobtainable, but noise levels near vents were up to a factor of 10 times those away from vents. The contamination from vehicle flow noise prevented more robust further analysis of the spectrum.

Summary of Field Observations

The high-amplitude, low-frequency noise observed at 21° N, if it is of hydrothermal origin, would have to be produced by pulsations of flow or large cavity resonance (or an unidentified mechanism) since sound source processes associated with turbulent jet flows would generate much higher frequencies than observed. However, the source must have been local to produce such large-amplitude variations over the relatively (as compared to the wavelength) short receiver spacing.

Noise measurements made in Axial Caldera 2 years earlier [*Bibee and Jacobson*, 1986] are comparable to the data from this experiment. The 1985 instrument placed closest to the vents detected sound about a factor of 10 in power lower than our lowest noise record. Anomalously high noise from the northern part of the caldera measured on the 1985 experiment remains unexplained, but in light of our experiment, it is not from a typical black smoker vent field like Ashes.

CONCLUSIONS

High-quality data collected on this experiment were used to characterize the noise field associated with Ashes Vent Field on Axial Seamount. Narrow band temporal variability was dominated by local ship traffic, submarines, and whales. Broadband variability is attributed to changes in distant shipping or propagation paths thereof and to changes in local weather.

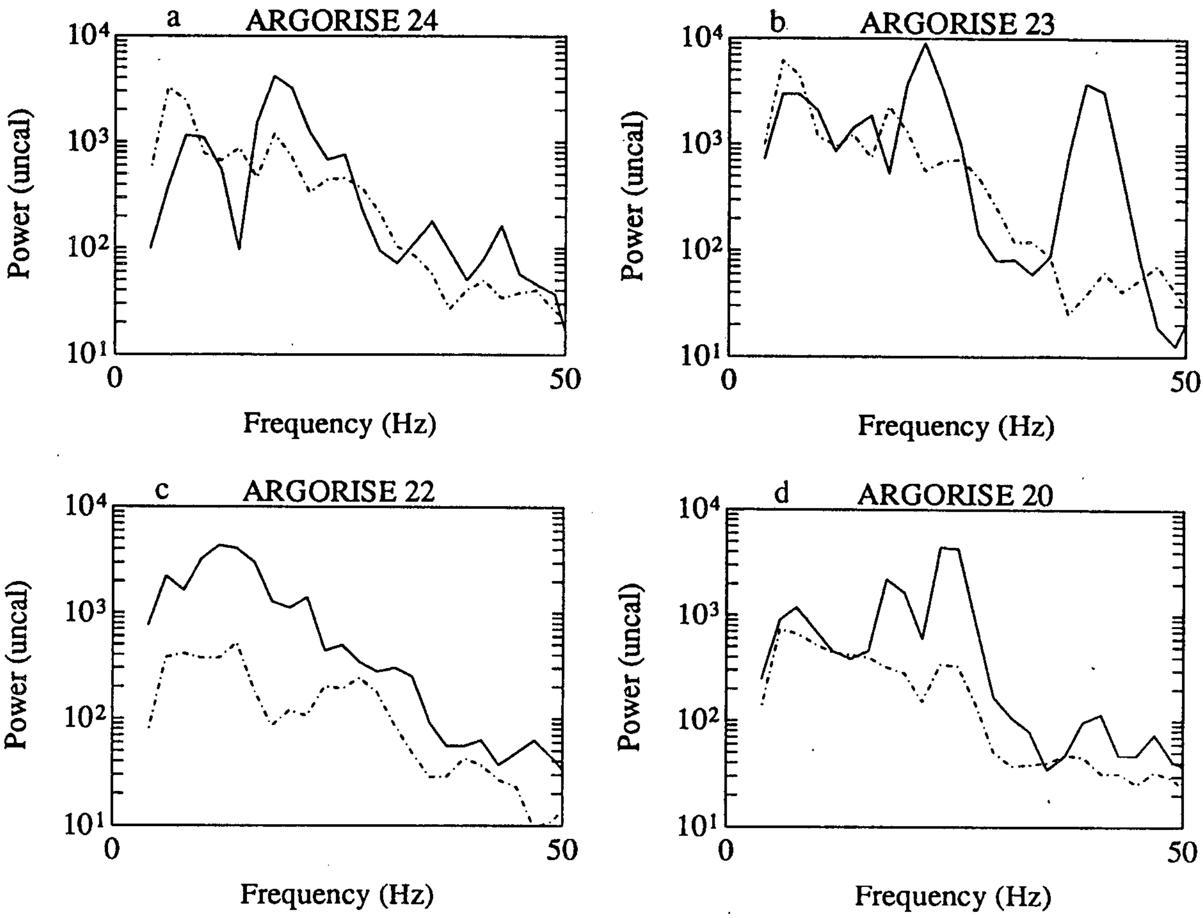

Fig. 30. Argo-Rise-towed hydrophone power spectra from four different deployments. Records taken within several meters of vents are in solid curves; those taken greater than 1 km are in dash-dotted curves. Power levels near vents are up to 10 times those away from vents in frequencies from 15 to 30 Hz. (*a*) ARGORISE 24, (*b*) ARGORISE 23, (*c*) ARGORISE 22, (*d*) ARGORISE 20.

The very low frequency signals (0.5-2 Hz) appear to be from two distinct sources, continuous microseisms and intermittent local events. Microseisms are equal in amplitude on both receivers and appear in almost all records. Sporadically appearing interface waves show high-pressure amplitudes near the seafloor and, decaying with vertical distance, produce very low signal levels at 40 m above the bottom. These may have been produced by magma or hydrothermal fluid movement.

No continuous vent signals were deemed significant based on a criterion of 90% probability of detection and 5% probability of false alarm. However, a small signal near 40 Hz, with a power level of 1×10^{-4} Pa^2/Hz was noticed on two records from the Inferno deployment. This frequency of this signal is consistent with predictions and the power level suggests the occurrence of jet noise amplification due to convected density inhomogeneities. The lack of higher signal levels precludes the presence of monopole (fluid pulsing) and dipole (chimney vibrations) sources in fluid flow associated with the chimneys.

Detection of vent signals was hampered by the unexpected spatial nonstationarity where receivers 38 m apart had about a factor 4 ambient noise level difference due to effects of local topography. This made absolute power level comparisons impossible, and the resulting low signal coherences reduced confidence in phase and directionality results.

Future experiments will need to include more receivers to improve the effective SNR. Several hydrophones should be located close enough to the vent (5 m) to allow beam forming through coherence and phase calculations. In addition, to improve SNR, a more active vent site should be chosen since acoustic power output increases rapidly with increasing fluid exit velocity.

To generalize from one vent site, it appears that the method of monitoring hydrothermal vent fluxes through passive acoustics will require more than a simple surface ship deployment of a two-element hydrophone array. It may be most useful on high output vent sites rather than on low to moderate hydrothermal areas.

APPENDIX A: THEORETICAL SOURCE MECHANISMS

Sound production in moving fluids may occur whenever there are pressure fluctuations, and these occur in all unsteady flows. Sometimes the pressure changes are associated with local fluctuations of mean or turbulent flow, and sometimes they propagate away from the flow as sound [*Ffowcs Williams*, 1969]. The propagating pressure field, or radiated far field, behaves as a classical acoustic wave whose speed depends on the compressibility of the fluid.

The basic physical processes which generate a radiating pressure field in a fluid primarily do so through mechanisms (Figure A1) described as monopoles, dipoles, and quadrupoles (or more generally, multipoles). The monopole radiator arises through volume or mass fluctuations, such as expanding and collapsing bubbles. The dipole radiator is generated by external force fluctuations, which result in variations of momentum, such as vibrations

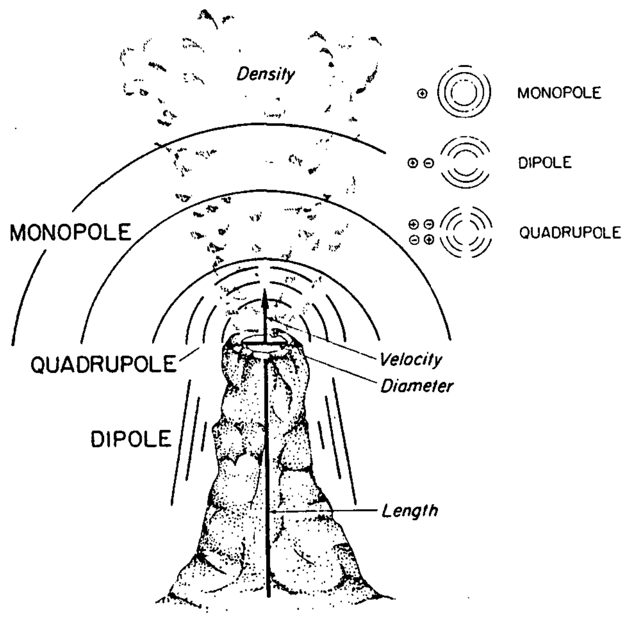

Fig. A1. Important jet sound generating parameters, including chimney length L, diameter D, exit velocity V_j, density ρ_j, and ambient density ρ_a, and monopole, dipole, and quadrupole source mechanisms.

of an object in a fluid. The quadrupole is produced by momentum fluctuations across a fixed surface, such as turbulent shear stress in the mixing region of a jet. In the mixing region of turbulent jets where shear stress is high, kinetic energy is converted to sound through changes in momentum flux. Quadrupole sources also can be considered to be formed by the opposing dipoles of vortices found on the edges of the jet [*Powell*, 1964].

Generally, multipole pressure fields may be divided into two regions of differing behavior. The near field is less than one wavelength from the source, and the far field is beyond one wavelength, although the change is not abrupt. A single monopole radiates a pressure wave equally in all directions. The amplitude decays as $1/r$, where r is radial distance from the source and it has no near field component. A dipole, made of two equal but opposite polarity monopoles, has a two-dimensional radiation pattern and is a less efficient radiator due to cancellation effects of the two monopoles. The near-field of a dipole, however, has a higher amplitude than that of a monopole of the same source strength and decays as $1/r^2$ until $r = \lambda$ (λ is wavelength). In the far field the amplitude of the dipole pressure wave decays as $1/r$. A quadrupole has a three-dimensional radiation pattern and, being formed from two equal but opposite dipoles, is the least efficient radiator. However, the near field of a quadrupole has the highest amplitude of these multipoles, and it decays as $1/r^3$. Its far field decays as $1/r$ but is the weakest of the three poles. Monopole radiation, if present, will dominate the far field acoustic signal, followed by dipole radiation. Quadrupole radiation will be significant only at high fluid exit velocities if the other sources are not present, or in the near field.

At hydrothermal vents it is possible that all three sources are present and that they are site specific. Monopole radiation can be produced by cavitation, boiling, pulsating exit flows, or resonance in subsurface cavities. Dipole radiation will arise from chimney resonace, interaction of the turbulent flow with a rigid surface, or convection of flow inhomogeneities. Quadrupole radiation will emanate from the shear stress produced in the turbulent mixing region of the free hydrothermal jet. Estimates of the contribution of these sources to a hydrothermal acoustic pressure field follow.

Sound production by hydrothermal vents is theoretically a function of fluid exit velocity V, temperature T, density ρ, sound speed c, orifice diameter D, and sulfide chimney dimension L, (for a one-phase fluid). The dependence of sound on these parameters varies according to the particular source mechanism involved. These parameters are difficult to measure and vary from site to site, but estimates have been obtained in several experiments [*Converse et al.*, 1984, *Little et al.*, 1987; *Tivey and Delaney*, 1986]. The following nominal values are used in this discussion of acoustic source mechanisms: velocity V = 2 m/s, temperature T = 350° C, density ρ = 1000 kg/m^3, orifice diameter D = 0.05 m, chimney length L = 3 m, sound speed c = 1500 m/s, and radial distance from source r=3 m.

We will examine theoretical sound levels based on these parameters for a variety of sound sources.

Monopole

Pulsating exit flow. The sound generated from the pulsating flow from a pipe can be treated as if it was produced by the motions of a baffled piston [*Ross*, 1976]. The pressure field from such a source is approximated as

$$P(r) \approx \frac{3\pi D P_p}{16r} \qquad (A1)$$

where P_p is the rms pressure fluctuation of pulsation. The total pressure produced by the mean flow of a jet is approximately ρV^2, where V is the mean exit velocity. If we assume that P_p is 10% of the mean flow, then

$$P(r) \approx \frac{3\pi D 0.1 \rho V^2}{16r} \qquad (A2)$$

Equation (A2) yields a nominal power level of P=16 Pa^2/Hz for pulsating exit flow.

Subsurface cavity resonance. Hydrothermal vents are generally found on fresh basalt flows, which often contain numerous drained lava lakes and collapse pits. Recent efforts to drill into zero-age crust at a hydrothermal site were hampered by the presence of subsurface cavities [*Ocean Drilling Program (ODP)*, 1986]. These cavities are capable of resonating and producing considerable sound if excited at the proper frequency. Fluid moving in and out of a cavity provides a driven mass, while the flexibility of the cavity walls provides the spring action to sustain resonance. Flow excitation of the cavity occurs through interaction of turbulent flow with the walls as the fluid enters the volume. If the dominant frequency of turbulence approaches the resonance frequency of the cavity, the cavity will begin to pulsate, which, in turn, will amplify production of that very frequency of turbulence [*Laufer and Yen*, 1983]. Such flow-excited resonance will radiate a strong tonal component [*Ross*, 1976]. The frequency of such acoustic radiation, being dependent on cavity size, rigidity, and geometry, is difficult to predict since very little information on subsurface cavity structure in hydrothermal systems exits. The magnitude of radiated power depends on how close the bandwidth of the excitation frequency is to the resonant frequency of the cavity. This type of sound would be extremely site specific in hydrothermal systems.

Cavitation. Cavitation is the formation of a macroscopic bubble at a liquid-liquid or liquid-solid interface caused by a local drop in pressure [*Ross*, 1976; *Urick*, 1975]. Such local pressure drops occur when a moving fluid is forced to accelerate around a bend or past a fixed object. The magnitude of this pressure drop is a function of the density and velocity of the fluid and is approximately equal to $\rho V^2/2$, which for hydrothermal vents is about 2000 Pa. Cavitation inception depends on the existence of submicroscopic voids, called cavitation nuclei, in the liquid. When pressure outside a nucleus drops below the surface tension of the bubble, rapid vaporization can occur and the bubble will rupture, expand, and then collapse, producing significant monopole sound. The rates of growth and collapse, which determine acoustic frequency and power, are affected by the interaction of the pressure and velocity fields at the moving boundary, surface tension, evaporation, dissolved gas content, heat conduction, viscosity and compressibility. Dissolved noncondensible gas in the fluid has the effect of cushioning the collapsing bubble, causing multiple rebounds, and reducing sound production.

The peak frequency of cavitation is inversely related to bubble radius α, which is likely to be small given the depth and large static pressure at vents,

$$f = \frac{1}{2\alpha}\sqrt{\frac{P}{\rho}} \tag{A3}$$

where

$$P = p(a) - p(\infty) \tag{A4}$$

$p(\infty)$ is ambient pressure, $p(a)$ is the pressure in the liquid just outside the liquid-gas surface, and ρ is ambient fluid density. Low-frequency, broadband noise dominates when the noncondensible gas content of the bubble is high. Sharp, high-amplitude peaks are characteristic of cavitation due to water vapor only. The inception of cavitation has been experimentally determined to depend on a cavitation parameter:

$$K = \frac{(P(\infty) - P_v - P_g)}{(0.5\rho V^2)} \tag{A5}$$

where P_v is vapor pressure in the bubble and P_g is gas pressure in the bubble. If K is greater than 4, cavitation will not occur [*Ross*, 1976]. Hydrothermal vents have been found at depths of 1500-3700 m, which correspond to ambient pressures of $1.5\mathrm{x}10^7$ - $3.7\mathrm{x}10^7$ Pa. The vapor pressure of seawater at 350° C is about $1.5\mathrm{x}10^7$ Pa. The dissolved gas content will effectively increase the pressure inside the bubble. It is therefore possible that cavitation occurs at shallow vent sites where $P(\infty) - P_v < 8000$ Pa. However, it is highly unlikely for cavitation to be a source of sound at greater depths.

Boiling. Boiling differs from cavitation in that the enlargement of bubbles occurs due to an increase in temperature and hence vapor pressure, rather than a decrease in local outside pressure. Sound production will depend on the temperature of the hydrothermal fluid and the depth of the vent. Most systems will not exhibit boiling at the vent orifice. However, some of the shallower vent sites could experience two-phase separation [*Delaney et al.*, 1983] and generate sound through growth and collapse of bubbles. This process, being monopole in nature, could be of primary importance in hydrothermal sound generation, if present. Recent studies north of Iceland (J. Olafsson, personal communication, 1988) have visually documented boiling at discharge sites of hydrothermal vents at a depth of 100 m. These vents will have a distinctive acoustic signature.

Dipole

Chimney vibrations. It is possible for turbulent flow through sulfide chimneys to induce vibrations in their structures. The frequency of oscillation depends on the stiffness and length of the chimney. The amplitude depends, as in cavity resonance, on mean flow velocity and on how close the forcing frequency is to the natural frequency of the chimney. A way to estimate pressure from a vibrating chimney is to use the general description of dipole resonance, coupled with a frequency estimate from theories of structural vibrations for circular beams [*Ross*, 1976]. The dipole source term D_o due to a fluctuating force F at frequency f is

$$D_o = \frac{F}{2\pi i f} \tag{A6}$$

Maximum pressure amplitude for dipole radiation is given by

$$P = \frac{-(2\pi f)^2 D_o}{4\pi r c} = \frac{2\pi i f F}{4\pi r c} \tag{A7}$$

The frequency of resonance in a circular beam is given by

$$f = \frac{(2m-1)\pi d c_b}{8\sqrt{8}L^2\sqrt{1+\frac{\rho}{\rho_b}}} \tag{A8}$$

where c_b is sound velocity in the beam, ρ_b is beam density, and d is beam diameter (=1 m). Using a value of c_b=3000 m/s, ρ_b = 4000 kg/m^3 and m=1, equation (A8) results in a frequency of 40 Hz. Force F is estimated by assuming that 10% of the available pressure from fluid flow (4000 Pa from above) acts upon the inside wall of the chimney of length L and diameter 0.05 m, which results in a force of approximately 240 N. Equations (A7) and (A8) yield a nominal power level for a vibrating chimney of P=1 Pa^2/Hz.

Quadrupole

Lighthill's [1952] formulation of the aeroacoustic problem (for a single-phase fluid) showed that the mixing region of a jet could be equated to a volume of quadrupoles with strength proportional to the stress tensor in the moving fluid. Such a mathematical formulation allows radiated jet acoustic power levels to be estimated and shown to be proportional to V^8 for low Mach number flow [*Lighthill*, 1952, 1954].

The frequency of jet noise depends, in part, on the size of the turbulent eddies in the jet, which scale with jet diameter [*Lighthill*, 1963]. Since the jet expands laterally and decreases speed with increasing distance from the orifice, acoustic power and frequency from a given section of jet will both decrease. The resultant far-field spectrum will have a peak frequency near $0.8V/D$ [*Lush*, 1971] with a power falloff of 6-9 dB per octave (frequency doubling) below the peak and 2-3 dB per octave above the peak. In the near field, the frequency spectrum produced will be similar but depend on relative proximity to either the mixing region near the orifice, which produces high frequencies, or the fully developed turbulent region farther downstream which produces lower frequencies.

The power and frequency distribution are both directional in jets, with higher frequencies being stronger at 90° to the jet axis and lower frequencies dominating at low angles (< 45°) to the jet axis [*Lush*, 1971].

Sound production by turbulent jets is a complicated process, and extensive theoretical and laboratory work has examined the exact directionality, frequency, and power of sound from low to high Mach number (M) jets [*Lighthill*, 1954; *Ffowcs Williams*, 1977; *Lush*, 1971; *Lauffer and Yen*, 1983; *Goldstein*, 1984; *Powell*, 1964; *Dowling et al.*, 1978; *Mankbadi*, 1985; *Cohen and Wygnaski*, 1987]. There are, however, very few experimental results on very low Mach number jets [*Jorgensen*, 1961]. Hydrothermal vents, with a nominal Mach number of M=10^{-3}(V = 1.5 m/s; c = 1500 m/s), fall into this category. Therefore we will use theoretical studies of jet radiation efficiency to predict intensity of jet noise from vents. The maximum pressure field of low Mach number jets in the far field is proportional to [*Lush*, 1971]

$$P \propto \frac{\rho V^4 D}{c^2 r} \tag{A9}$$

at a peak frequency of

$$f \approx \frac{V}{D} \tag{A10}$$

The absolute magnitude of the near and far pressure fields of a turbulent jet generating quadrupole radiation can be approximated by [*Ross*, 1976; J. E. Ffowcs Williams, personal communication, 1988]:

$$P = 10^{-2} \rho V^2 \qquad \text{for} \qquad r < D \tag{A11}$$

$$P = 10^{-2} \rho V^2 (\frac{D}{r})^3 \qquad \text{for} \qquad r < \lambda \tag{A12}$$

$$P = 10^{-2} \rho V^2 (\frac{D}{\lambda})^2 \frac{D}{r} \qquad \text{for} \qquad r > \lambda \tag{A13}$$

The nominal near field quadrupole power level is 4×10^{-8} Pa^2/Hz, and the corresponding far field power is 2×10^{-12} Pa^2/Hz.

Other Effects

Pipe resonance. Flow through a hydrothermal chimney can set up resonant internal pressure waves, much like an organ pipe, whose frequency depends on sound speed in the fluid and on the length of the pipe:

$$f = \frac{nc}{L} \tag{A14}$$

where n is an integer. Power level depends in part on how similar the frequency of the driving pressure oscillations are to the resonant frequencies of the pipe, and is difficult to predict in hydrothermal systems since nothing is yet known about variations in fluid flow.

Flow inhomogeneities. If a turbulent flow is of non-uniform density, the most efficient source is not the velocity quadrupole term but a dipole order term whose radiated power scales as V^6 [*Morfey*, 1973]. This is due to the fact that accelerated density differences found in heterogeneous turbulent flow are effectively force fluctuations resulting in variations of momentum, which radiate as more efficient dipoles. The radiation efficiency of this type of flow is represented by a ratio of dipole pressure, P_d field to quadrupole pressure field P_q [*Morfey*, 1973]:

$$\frac{P_d}{P_q} = \frac{c \rho D_v}{V} \tag{A15}$$

where D_v is the specific volume difference between jet and ambient fluid. The amplification is inversely proportional to Mach number and, as such, may be a very strong effect at hydrothermal vents. For hydrothermal fluid at 350° C, the specific volume difference is approximately 0.5×10^{-3} kg/m^3, and

$$\frac{P_d}{P_q} = 4 \times 10^2 \tag{A16}$$

Summary

The complexities and variability of hydrothermal vent systems allow for a wide range of possible sound generating mechanisms. Nominal sound power levels indicate that some vents may produce significantly more sound than others based on geometry and structure alone, with lower-order modes dominating, if present. In addition, the range of velocities seen at vents will give rise to an additional several orders of magnitude range in power levels as most mechanisms are heavily dependent on velocity. This theoretical analysis suggests that monitoring changes in vent fields through sound is feasible, although specific sources and power levels may vary considerably depending on vent site. On the other hand, determining exact values for velocity, diameter, length, and temperature will depend so heavily on chimney dimensions and internal structure that a complete morphologic description of the vent field would be required to separate out the different source mechanisms.

APPENDIX B

The signal detection ability of a hydrophone array in a noise field is calculated by determining the raw input signal level required to achieve a given probability of detection while maintaining an acceptable probability of false alarm. The probability of detecting a signal within a gaussian noise distribution depends on the amplitude of the signal, amplitude, and coherence length of noise, number of observations, and number of receivers.

A matrix description P_f of the signal waveform for a receiver array with a point source located at the hydrothermal chimney orifice, can be generated from a description of the waveform at each receiver [from *Owsley and Swope*, 1981], V_f:

$$V_f = [a_1 e^{-j2\pi f r_1/c}, a_2 e^{-j2\pi f r_2/c}] \tag{B1}$$

Here f is frequency, j is $\sqrt{-1}$, r_1 and r_2 are receiver-source separation distances for the upper and lower hydrophones, c is sound speed and a is an amplitude factor accounting for spherical spreading loss:

$$a_i = 1/r_i \tag{B2}$$

and,

$$P_f = V_f V_f^+ \tag{B3}$$

The correlation length of the ambient noise field in the ocean will determine how difficult noise removal will be given a fixed receiver separation. We will assume that the noise field is isotropic both for simplicity and since the results are not significantly different from either surface generated or azimuthally distributed noise fields. For isotropic noise, the correlation function q is [*Burdick*, 1984]

$$q = \frac{\sin(2\pi d/\lambda)}{2\pi d/\lambda} \tag{B4}$$

where d is receiver separation and λ is wavelength. The array noise correlation function for two receivers will then be

$$Q_f = \begin{pmatrix} 1 & q \\ q & 1 \end{pmatrix} + \epsilon \begin{pmatrix} 1 & 0 \\ 0 & 1 \end{pmatrix} \tag{B5}$$

where ϵ is zero for perfectly bandlimited, perfectly predictable noise, but for real, ocean systems with a random uncorrelated noise component, ϵ must be nonzero. For isotropic noise, ϵ is approximated by 0.1 (J. Krolik, personal communication, 1988).

The effective signal-to-noise ratio output (SNR_o) of a system in a coherent noise field is [from *Bangs and Schultheiss*, 1973]

$$SNR_o = N \sum_{f=1}^{f} (S_f/N_f)^2 \text{trace}[(P_f Q_f^{-1})^2] \tag{B6}$$

where N is number of sample sets and S_f/N_f is the SNR as a function of frequency input to each receiver. Equation (B6) is used to calculate the output SNR_o given an input S_f/N_f. For the 100-Hz bandwidth, S_f/N_f is calculated using an average of the quietest records from the lower hydrophone of the opposite deployment as the value of ambient noise N_f. This must be done because the upper hydrophone of both deployments had such high noise levels. The assumption inherent in this procedure is that the two vents are not producing exactly the same signal. The SNR_o is then calculated in 5.3-Hz frequency bands. The SNR_o equals *Burdick*'s [1984] detectability index d_o. We have chosen as significant a d_o greater than 10, which is equivalent to a probability of detection of 90% and a probability of false alarm of 5% [*Burdick*, 1984].

Acknowledgements. The successful completion of the field experiment was due in a large part to the generous help of C. Fox, H. Milburn, E. Mellinger, the officers and crew of *Atlantis II*, the *Alvin* group, and the NOAA Vents personnel. C. Bradley's aid in the analysis of the interface waves was very useful and much appreciated. R. Ballard provided the technical and field support for the Argo-Rise cruise. The Department of Mathematics, University of Western Australia generously provided support for publishing this paper. This work was supported by the WHOI/MIT Education Office, NOAA National Sea Grant College Progam Office, Deptartment of Commerce under grant NA86-AA-D-SG090, WHOI Sea Grant (R/6-14), the Office of Naval Research grant N00014-87-K-0007, and the NOAA Vents Program. WHOI contribution number 7122.

REFERENCES

Akal, T., A. Barbagelata, G. Giudi, and M. Snoek, Time dependence of infrasonic ambient seafloor noise on a continental shelf, in *Ocean Seismo-Acoustics: Low-Frequency Underwater Acoustics*, edited by T. Akal and J.M. Berkson, pp. 767-778, Plenum, New York, 1986.

Argo-Rise Group, Geological mapping of the East Pacific Rise axis (10° 19' - 11° 53'N) using the Argo and ANGUS imaging systems, *Canad. Mineral.*, *26*, 467-486, 1988.

Ballard, R. D., J. Francheteau, C. Rangan, and W. Normark, East Pacific Rise at 21° N: The volcanic, tectonic and hydrothermal processes at the central axis, *Earth Planet. Sci. Lett.*, *55*, 1-10, 1981.

Ballard, R.D., T. H. Van Andel, and R. T. Holcomb, The Galapagos Rift at 86° W, 5, Variations in volcanism, structure, and hydrothermal activity along a 30-km segment of the rift valley, *J. Geophys. Res.*, *87*, 1149-1161, 1982.

Ballard, R.D., R. Hekinian, and J. Francheteau, Geological setting of hydrothermal activity at 12° 50'N on the East Pacific Rise: A submersible study, *Earth Planet. Sci. Lett.*, *69*, 176-186, 1983.

Bangs, W.J., and P.M. Schultheiss, Space-time processing for optimal parameter estimation, *Signal Processing*, edited by J.W.R Griffiths, P.L. Stocklin, and C. van Schooneveld, pp. 577-590, Academic, San Diego, Calif., 1973.

Bibee, L.D., and R.S. Jacobson, Acoustic noise measurements on Axial Seamount, Juan de Fuca Ridge, *Geophys. Res. Lett.*, *13*(9), 957-960, 1986.

Burdick, W.S., *Underwater Acoustic System Analysis*, chap. 10, Prentice-Hall, Englewood Cliffs, N.J., 1984.

Canadian American Seamount Expedition, Hydrothermal vents and sulfide deposits, Axial Seamount, Juan de Fuca Ridge, *Proc. Oceans '83*, 801, 1983.

Canadian American Seamount Expedition, Hydrothermal vents on an axis seamount of the Juan de Fuca Ridge, *Nature*, *313*, 212-214, 1985.

Cann, J.R., and M.R. Strens, Black smokers fuelled by freezing magma, *Nature*, *298*, 147-149, 1982.

Cann, J.R., M.R. Strens, and A. Rice, A simple magma-driven thermal balance model for the formation of volcanogenic massive sulphides, *Earth Planet. Sci. Lett.*, *76*, 123-134, 1986.

Chase, R.L., R.R. Delaney, H.P. Johnson, S.K. Juniper, J.L. Karsten, J.E. Lupton, S.D. Scott, and V. Tunnecliffe, North caldera hydrothermal vent field, Axial Seamount, Juan de Fuca Ridge (abstract), *Eos Trans. AGU*, *64*, 723, 1983.

Cohen, J., and I. Wygnanski, The evolution of instabilities in the axisymmetric jet, part 1, The linear growth of disturbances near the nozzle, *J. Fluid Mech.*, *176*, 191-219, 1987.

Converse, D.R., H.D. Holland, and J. Edmond, Flow rates in the axial hot springs of the East Pacific Rise (21° N): Implications for the heat budget and the formation of massive sulfide deposits, *Earth Planet. Sci. Lett.*, *69*, 159-175, 1984.

Corliss, J.B., J. Dymond, L.I. Gordon, J.M. Edmond, R.P. Von Herzen, R.D. Ballard, K. Green, D. Williams, A. Bainbridge, K. Crane, and T.H. van Andel, Submarine thermal springs on the Galapagos Rift, *Science*, *203*, 1073-1083, 1979.

Craig, H.,V.K. Craig, and K.-R. Kim, PAPATUA Expedition, I, Hydrothermal vent surveys in back-arc basins: The Lau, N. Fiji, Woodlark, and Manus Basins and Havre Trough (abstract), *Eos Trans. AGU*, *68*, 100, 1987.

Crane, K., F. Aikman, R. Embley, S. Hammond, A. Malahoff, and J. Lupton, The distribution of geothermal fields on the Juan de Fuca Ridge, *J. Geophys. Res.*, *90*, 727-744, 1985.

Delaney, J.R., and B.A. Cosens, Boiling and metal deposition in submarine hydrothermal systems, *Mar. Technol. Soc. J.*, *16*(3), 62-65, 1983.

Dowling, A.P., and J.E. Ffowcs Williams, *Sound and Sources of Sound*, p. 95, Ellis Horwood, Chichester, 1983.

Dowling, A.P., J.E. Ffowcs Williams, and M.E. Goldstein, Sound production in a moving stream, *Philos. Trans. R. Soc. London, Ser. B*, *288*, 321-349, 1978.

Embley, R.W., S.R. Hammond, and K. Murphy, The caldera of Axial Volcano: remote sensing and submersible studies of a hydrothermally active submarine volcano, *NOAA Symp. Ser. Undersea Res.*, *6*(2), 1988.

Ffowcs Williams, J.E., Hydrodynamic noise, *Annu. Rev. Fluid Mech.*, *1*, 197-222, 1969.

Ffowcs Williams, J.E., Aeroacoustics, *Annu. Rev. Fluid Mech.*, *9*, 447-468, 1977.

Francheteau, J., and R.D. Ballard, The East Pacific Rise near 21° N, 13° N, and 20° S: Inferences for along-strike variability of axial processes of the mid-ocean ridge, *Earth Planet. Sci. Lett.*, *64*, 93-116, 1983.

Goldstein, M.E., Aeroacoustics of turbulent shear flows, *Annu. Rev. Fluid Mech.*, *16*, 263-285, 1984.

Hammond, S.R., et al., Pisces submersible exploration of a high-temperature vent field in the caldera of Axial Volcano, Juan de Fuca Ridge (abstract), *Eos Trans. AGU*, *67*, 1027, 1986.

Hammond, S.R., J.S. Lee, A. Malahoff, R. Feeley, R.W. Embley, and J. Franklin, Discovery of high-temperature hydrothermal venting on the Endeavor Segment of the Juan de Fuca Ridge (abstract), *Eos Trans. AGU*, *65*, 1111, 1984.

Hekinian, R., J. Francheteau, V. Renard, R.D. Ballard, P. Choukroune, J.L. Cheminee, F. Albarede, J.F. Minster, J.C. Marty, J. Boulegue, and J.L. Charlou, Intense hydrothermal activity at the axis of the East Pacific Rise near 13° N: Submersible witness of the growth of sulphide chimney, *Mar. Geophys. Res.*, *6*, 1-14, 1983.

Hessler, R.R., and W.M. Smithey, The distribution and community structure of megafauna at the Galapogos hydrothermal vents, edited by P.A. Rona, K. Bostrom, L. Laubier, and K. Smith, *Hydrothermal Processes at Sea-floor Spreading Centers*, pp. 735-770, Plenum, New York, 1983.

Hessler, R.R., W.M. Smithey, and C.H. Keller, Spatial and temporal variation of giant clams, tube worms and mussels at deep-sea hydrothermal vents, Hydrothermal Vents of the Eastern Pacific: An Overview, edited by M.L. Jones, *Bull. Biol. Soc. Wash.*, *6*, 411-428, 1985.

Hoagland, P., and J. Broadus, Seabed material commodity and resource summaries, *Tech. Rep. WHOI-87-43*, pp. 97-125, Woods Hole Oceanogr. Inst., Woods Hole, Mass., 1987.

Hodgkiss, W.S., and V.C. Anderson, Detection of sinusoids in ocean acoustic background noise, *J. Acoust. Soc. Am.*, *67*(1), 214, 1980.

Johnson, P.H., and V. Tunnecliffe, Time-series measurements of hydrothermal activity on northern Juan de Fuca Ridge, *Geophys. Res. Lett.*, *12*(10), 685-688, 1985.

Jorgensen, D., "Near field" noise from turbulent jets, *J. Acoust. Soc. Am.*, *33*(6), 817, 1961.

Karsten, J., et al., Regional setting and local character of a hydrothermal field/sulfide deposit on the Endeavor Segment of the Juan de Fuca Ridge (abstract), *Eos Trans. AGU*, *65*, 1111, 1984.

Laufer, J., and T. Yen, Noise generation by a low-Mach number jet, *J. Fluid Mech.*, *134*, 1-31, 1983.

Lighthill, M.J., On sound generated aerodynamically, I, General theory, *Proc. R. Soc. London, Ser. A*, *211*, 564-587, 1952.

Lighthill, M.J., On sound generated aerodynamically, II, Turbulence as a source of sound, *Proc. R. Soc. London*, *222*, 1-32, 1954.

Lighthill, M.J., Jet noise, *AIAA J.*, *1*(7), 1507-1517, 1963.

Little, S.A., K.D. Stolzenbach, and R.P. Von Herzen, Measurements of plume flow from a hydrothermal vent field, *J. Geophys. Res.*, *92*, 2587-2596, 1987.

Little, S.A., K.D. Stolzenbach, and F.J. Grassle, Tidal current effects on temperature in diffuse hydrothermal flow, Guaymas basin, *Geophys. Res. Lett.*, *15*(13), 1491-1494, 1988.

Lush, P.A., Measurements of subsonic jet noise and comparison with theory, *J. Fluid Mech.*, *46*, 477-500, 1971.

Macdonald, K.C., A geophysical comparison between fast and slow spreading centers: constraints on magma chamber formation and hydrothermal activity, *Hydrothermal Processes at Sea-floor Spreading Centers*, pp. 27-51, edited by P.A. Rona, K. Bostrom, L. Laubier, and K. Smith, Plenum, New York, 1983.

Mankbadi, R.R., On the interaction between fundamental and subharmonic instability waves in a turbulent round jet, *J. Fluid Mech.*, *160*, 385-419, 1985.

McConachy, T.F., R.D. Ballard, M.J. Mottl, and R.P. Von Herzen, Geologic form and setting of a hydrothermal vent field at lat 10° 56'N, East Pacific Rise: A detailed study using Angus and Alvin, *Geology*, *14*, 295-298, 1986.

Mellinger, E.C., K.E. Prada, R.L. Koehler, and K.W. Doherty, Instrument Bus an electronic system architecture for oceanographic instrumentation, *Tech. Rep. WHOI-86-30*, Woods Hole Oceanogr. Inst., Woods Hole, Mass., 1986.

Morfey, C.L., Amplification of aerodynamic noise by convected flow inhomogeneities, *J. Sound Vib.*, *31*(4), 391-397, 1973.

Normark, W.R., et al., Active hydrothermal vents and sulfide deposits on the southern Juan de Fuca Ridge, *Geology*, *11*, 158-163, 1986.

Ocean Drilling Program Leg 106 Scientific Party, Drilling the Snake Pit hydrothermal sulfide deposit on the Mid-Atlantic Ridge, lat. 23° N, *Geology*, *14*, 1004-1007, 1986.

Oppenheim, A.V., and R.W. Schafer, *Digital Signal Processing*, Prentice-Hall, Englewood Cliffs, N. J., 1975.

Owsley, N.L., and G.R. Swope, Time delay estimation in a sensor array. *IEEE Trans. Acoust. Speech Signal Process.*, *ASSP29*(3), 519-523, 1981.

Powell, A., Theory of vortex sound, *J. Acoust. Soc. Am.*, *36*, 1, 1964.

Riedesel, M., J.A. Orcutt, K.C. Macdonald, and J.S. McClain, Microearthquakes in the black smoker hydrothermal field, East Pacific Rise at 21° N, *J. Geophys. Res.*, *87*, 10,613-10,623, 1982.

Rona, P.A., G. Thompson, M.J. Mottl, J.A. Karson, W.J. Jenkins, D. Graham, M. Mallette, K. Von Damm, and J.M. Edmond, Hydrothermal activity at the TAG hydrothermal field, Mid-Atlantic Ridge crest at 26° N, *J. Geophys. Res.*, *89*, 11,365-11,377, 1984.

Ross, D., *Mechanics of Underwater Noise*, Pergamon, New York, 1976.

Scott, S.D., T.J. Barrett, M. Hannington, R.L. Chase, Y. Fouquet, and K. Juniper, Tectonic framework and sulfide deposits of Southern Explorer Ridge, northeastern Pacific Ocean (abstract), *Eos Trans. AGU*, *65*, 1111, 1984.

Tivey, M.K., and J.R. Delaney, Growth of large sulfide structures on the Endeavour Segment of the Juan de Fuca Ridge, *Earth Planet. Sci. Lett.*, *77*, 303-317, 1986.

Urick, R.J., *Principles of Underwater Sound for Engineers*, 2nd ed., McGraw-Hill, New York, 1975.

Urik, R.J., *Ambient Noise in the Sea*, Peninsula, Los, Altos, 1986.

Van Dover, C.L., A comparison of stable isotope ratios ($^{18}O/^{16}O$ and $^{13}C/^{12}C$) between two species of hydrothermal vent decapods (Alvinocaris lusca and Munidopsis subsquamosa), *Mar. Ecol.*, *31*, 295-299, 1986.

Watkins, W.A., Activities and underwater sounds of fin whales, *Sci. Rep. Whales Res. Inst.*, *33*, 83-117, 1981.

Webb, S.C., Observations of seafloor pressure and electric field fluctuations, Ph.D. thesis, Scripps Inst. Oceanogr., Univ. of Calif., San Diego, La Jolla, 1984.

Wentz, G.M., Acoustic ambient noise in the ocean: Spectra and sources, *J. Acoust. Soc. Am.*, *34*, 1936-1956, 1962.

S. A. Little, 37 Conant Rd. Lincoln, MA 01773.

G. M. Purdy, Department of Geology and Geophysics, Woods Hole Oceanographic Institution, Woods Hole, MA 02554.

K. D. Stolzenbach, Department of Civil Engineering, Ralph Parson's Laboratory, Massachusetts Institute of Technology, Cambridge, MA 02139.

(Received April 10, 1989;
revised November 24, 1989;
accepted December 12, 1989.)